



Discovery of a potent dual inhibitor of wild-type and mutant respiratory syncytial virus fusion proteins through the modulation of atropisomer interconversion properties

Toru Yamaguchi-Sasaki^{a,*}, Takanori Kawaguchi^a, Atsushi Okada^b, Seiken Tokura^b, Nozomi Tanaka-Yamamoto^a, Tomoki Takeuchi^a, Yuya Ogata^a, Ryo Takahashi^a, Risa Kurimoto-Tsuruta^a, Tomokazu Tamaoki^a, Yutaka Sugaya^c, Tomoko Abe-Kumasaka^c, Kaho Arikawa^c, Ippei Yoshida^c, Hiroyuki Sugiyama^c, Kosuke Kanuma^a, Mitsukane Yoshinaga^a

^a Medicinal Chemistry Laboratories, Taisho Pharmaceutical Co., Ltd., 1-403 Yoshino-cho, Kita-ku, Saitama 331-9530, Japan

^b Discovery Technologies Laboratories, Taisho Pharmaceutical Co., Ltd., 1-403 Yoshino-cho, Kita-ku, Saitama 331-9530, Japan

^c Pharmacology Laboratories, Taisho Pharmaceutical Co., Ltd., 1-403 Yoshino-cho, Kita-ku, Saitama 331-9530, Japan

ARTICLE INFO

Keywords:

Respiratory syncytial virus
Fusion protein
Pyrazolo[1,5-a]pyrimidines
Atropisomer
Macrocyclic

ABSTRACT

The development of effective respiratory syncytial virus (RSV) fusion glycoprotein (F protein) inhibitors against both wild-type and the D486N-mutant F protein is urgently required. We recently reported a 15-membered macrocyclic pyrazolo[1,5-a]pyrimidine derivative **4** that exhibited potent anti-RSV activities against not only wild-type, but also D486N-mutant F protein. However, NMR studies revealed that the 15-membered derivative **4** existed as a mixture of atropisomers. An optimization study of the linker moiety between the 2-position of the benzoyl moiety and the 7-position of the pyrazolo[1,5-a]pyrimidine scaffold identified a 16-membered derivative **42c** with an amide linker that showed a rapid interconversion of atropisomers. Subsequent optimization of the 5-position of the pyrazolo[1,5-a]pyrimidine scaffold and the 5-position of the benzoyl moiety resulted in the discovery of a potent clinical candidate **60b** for the treatment of RSV infections.

1. Introduction

Human respiratory syncytial virus (RSV) is an RNA virus that is classified into the *Paramyxovirus* genus in the family *Pneumoviridae*.¹ The most common disorder caused by human RSV infection is lower respiratory tract infections, such as asthma, pneumonia, and severe bronchiolitis,²⁻⁸ particularly in infants and young children.⁹ While symptoms of RSV infection are relatively mild in normal adults and older children, people with underlying chronic respiratory or heart disease and immunocompromised patients are more prone to serious illness.^{10,11} Severe RSV infection often causes bronchitis and pneumonia, leading to increased mortality. Currently, RSV has spread all over the world and repeatedly infects humans throughout life.

According to a global systematic review, 33.1 million RSV-related acute lower respiratory tract infection (RSV-ALRI) episodes resulted in approximately 3.2 million hospitalizations and 59,600 in-hospital deaths in 2015.¹² Despite the mortality rate being higher for RSV infection than for influenza,¹³ no effective treatment for RSV infection currently exists other than supportive care.¹⁴⁻¹⁷ Two drugs, palivizumab (Synagis®) and ribavirin (Virazole®), have been approved for the treatment of RSV infections. Palivizumab is a humanized monoclonal antibody that inhibits infection by binding to a fusion glycoprotein (F protein) and blocking the binding or fusion of the virus to the host cell.^{14,15,18-21} Not only is the use of palivizumab restricted to prophylaxis in high-risk infants, but it is also very expensive. Ribavirin is an antiviral agent that has a wide range of antiviral and

Abbreviations: Boc, *tert*-butoxycarbonyl; Cbz, benzyloxycarbonyl; CDI, 1,1'-carbonyldiimidazole; CPE, cytopathic effect; CYP, cytochrome P450; DMA, dimethylacetamide; DMAP, 4-(*N,N*-dimethylamino)pyridine; EXSY, exchange spectroscopy; HATU, 1-[bis(dimethylamino)methylene]-1*H*-1,2,3-triazolo[4,5-*b*]pyridinium 3-oxide hexafluorophosphate; MDI, metabolism-dependent inhibition; Ms, methanesulfonyl; NMP, *N*-methylpyrrolidone; NMR, nuclear magnetic resonance; PAMPA, parallel artificial membrane permeability assay; PdCl₂(dppf), [1,1'-bis(diphenylphosphino)ferrocene]dichloropalladium(II); RSV, respiratory syncytial virus; SAR, structure-activity relationship; TBAF, tetrabutylammonium fluoride; TBS, *tert*-butyldimethylsilyl; TFA, trifluoroacetic acid; TMSCl, chlorotrimethylsilane.

* Corresponding author.

<https://doi.org/10.1016/j.bmc.2020.115818>

Received 7 August 2020; Received in revised form 26 September 2020; Accepted 5 October 2020

Available online 31 October 2020

0968-0896/© 2020 Elsevier Ltd. All rights reserved.

immunomodulatory effects on DNA or RNA viruses, but its use is limited because of concerns regarding efficacy and toxicity.^{22–28}

The RSV F protein plays a critical role in the fusion of the RSV envelope membrane and the host cell membrane, making it an attractive target for anti-RSV drug development. Several classes of compounds, such as pyrazolo[1,5-*a*]pyrimidines,^{29–32} benzimidazoles,^{33–35} and piperazinyl-quinolines,³⁶ have been developed as RSV F protein inhibitors. Among these compounds, a pyrazolo[1,5-*a*]pyrimidine derivative, presatovir (GS-5806, **1**), showed potent anti-RSV effects in clinical trials and achieved proof of concept in human RSV challenge studies.²⁹ In clinical trials, several presatovir-resistant mutants of RSV F protein have been isolated.^{37,38} Among them, the D486N mutant has been shown to exhibit cross-resistance to compounds with various chemical structures, such as MDT-637 (**2**) and TMC-353121 (**3**).^{39,40} We recently reported a potent RSV inhibitor **4** that was effective against not only wild-type, but also D486N-mutant F protein, the latter of which is of potential concern for human health.⁴¹ The improvement of anti-RSV activity against the D486N mutant was achieved by cross-linking the 2-position of the benzoyl moiety in **4** with the 7-position of the pyrazolo[1,5-*a*]pyrimidine scaffold, which constrains the conformation. However, compounds with a 15-membered macrocyclic ring have been found to consist of a mixture of atropisomers, as shown by NMR studies (Table 1). Atropisomers are classified into three classes based on their rotational energy barriers and interconversion rates, and these classes affect the difficulty of drug development.⁴² Class 2 compounds with interconversion half-lives ranging from minutes to days or months can be complicated to develop because of the difficulty in quantitatively determining the atropisomeric ratio over the time course of drug production and patient administration and the half-life in vivo. In fact, no class 2 drugs have been launched recently.^{43,44} Therefore, further optimization of **4** was needed to obtain a developable drug candidate with no atropisomer issues. There are three general strategies for avoiding atropisomers: 1) increasing the interconversion rate between conformations with barriers to rotation around the chiral axis (transforming the compound to class 1, with a rotation half-life of less than a few seconds); 2) freezing the rotation (transforming the compound to class 3, with a half-life of several years or longer); and 3) eliminating the chiral axis through symmetrization around the axis. In the case of our macrocyclic derivatives, the steric hindrance to rotation of the amide bond between the piperidine ring and the aryl group was considered to afford configurationally stable class 2 atropisomers. To avoid the formation of class 2 atropisomers by increasing the rate of rotation around the amide bond, the linker moiety connecting the 2-position of the benzoyl moiety to the 7-position of the pyrazolo[1,5-*a*]pyrimidine scaffold required optimization. The anti-RSV activity was also expected to be improved by optimizing the linker moiety, since the linker moiety is involved in the interaction with F protein.⁴¹ In the present paper, we describe the synthesis and optimization of the linker moiety of macrocyclic pyrazolo[1,5-*a*]pyrimidine derivatives without the formation of class 2 atropisomers and the further optimization of substituents on the

pyrazolo[1,5-*a*]pyrimidine and benzene ring to obtain orally available anti-RSV agents (see Fig 1).

2. Chemistry

First, a series of linker parts (**7**, **11**, **17**) were synthesized as shown in Scheme 1. Compound **6** was synthesized by the addition reaction of methyl 5-fluoro-2-hydroxybenzoate with an *O*-mesylated derivative of **5**, followed by the removal of the *tert*-butoxycarbonyl (Boc) group to obtain linker part **7**. In a similar manner, an intermediate **9** was synthesized by the substitution reaction of methyl 5-fluoro-2-hydroxybenzoate with an *O*-mesylated derivative of **8**. After the methylation of the nitrogen atom of **9** using iodomethane and silver oxide, the Boc group was removed to obtain linker part **11**. Compound **13** was prepared by an S_N2 reaction between 2-bromoethoxy-*tert*-butyldimethylsilyl-ane and *tert*-butyl *N*-(2-aminoethyl)-*N*-methylcarbamate **12**. Compound **15** was synthesized by protecting the secondary amine **13** with a Cbz group and removing the *tert*-butyldimethylsilyl (TBS) group with tetrabutylammonium fluoride (TBAF). Linker part **17** was prepared from **15** using the same synthetic method as that described for **7**.

Scheme 2 shows the synthesis of amide-type linker parts (**23a–c**, **28**). After the alkylation of phenols **19a–c** with *tert*-butyl 2-bromoacetate **18**, carboxylic acids **21a–c** were obtained by removing the *tert*-butyl group. The amidation of carboxylic acids **21a–c** with *tert*-butyl *N*-(2-aminoethyl)-*N*-methyl-carbamate and the subsequent removal of the Boc group provided linker parts **23a–c**. Amine **26** was obtained by the alkylation of methyl 5-fluoro-2-hydroxybenzoate with benzyl *N*-(2-bromoethyl)carbamate **24** and deprotection of the Cbz group. The amidation of amine **26** and 2-[*tert*-butoxycarbonyl(methyl)amino]acetic acid and the subsequent removal of the Boc group afforded linker part **28**.

Scheme 3 shows the synthesis of the linker parts with amide isosteres (**31**, **37**). *tert*-Butyl *N*-(2-aminoethyl)-*N*-methylcarbamate **12** was treated with chloromethanesulfonyl chloride and then reacted with methyl 5-fluoro-2-hydroxybenzoate to obtain **30**; the subsequent deprotection of the Boc group yielded linker part **31**. Methyl 2-(*tert*-butoxycarbonylamino)-3,3,3-trifluoropropanoate **32** was reduced to yield **33**; the hydroxyl group of **33** was mesylated, followed by alkylation with methyl 5-fluoro-2-hydroxybenzoate and deprotection of the Boc group to obtain **35**. After reductive amination with *tert*-butyl *N*-methyl-*N*-(2-oxoethyl)carbamate, the Boc group of **36** was removed to obtain linker part **37**.

The synthesis of macrocyclic derivatives **42a–i** is shown in Scheme 4. The pyrazolo[1,5-*a*]pyrimidine part **38**, which was prepared as described in our previous paper,⁴¹ was aminated with the linker parts (**7**, **11**, **17**, **23a–c**, **28**, **31**, **37**) prepared as shown above, hydrolyzed, and subjected to intramolecular condensation under a high-dilution condition to yield macrocyclic compounds **41a–i**. Finally, the desired macrocyclic products **42a–i** were synthesized by introducing an azetidine under microwave irradiation and basic conditions.

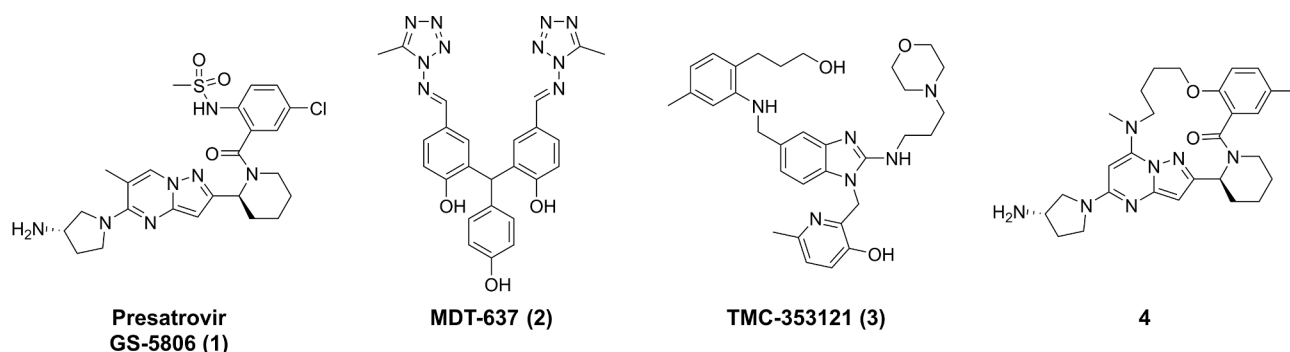
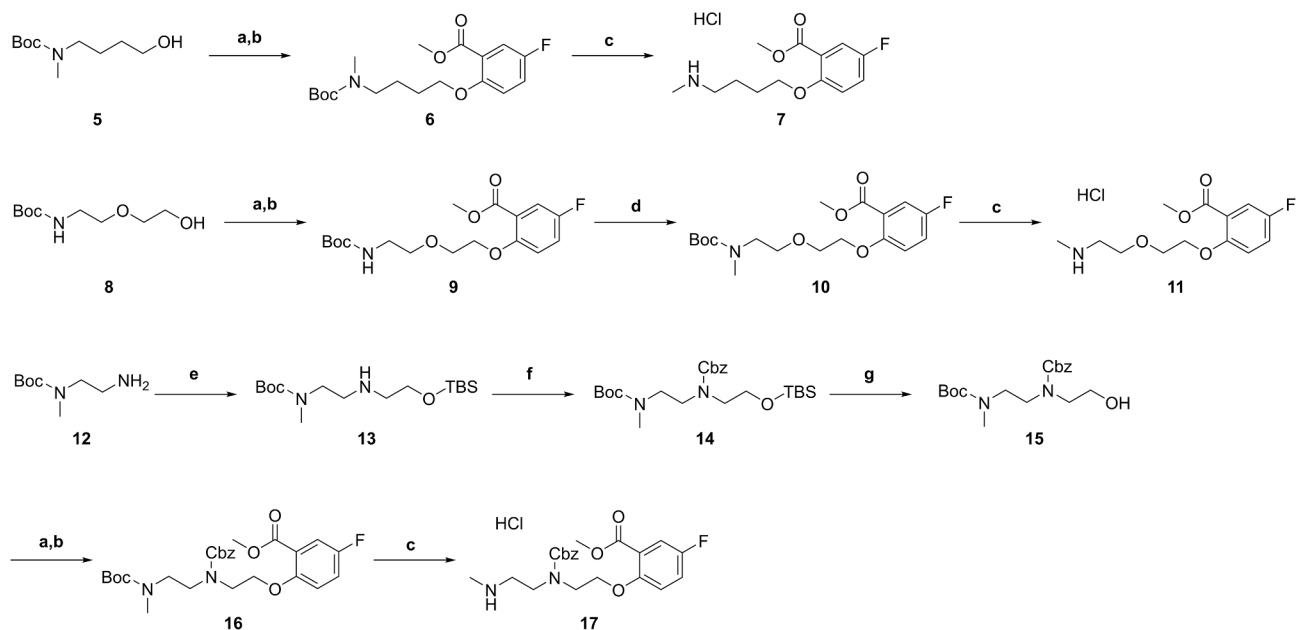
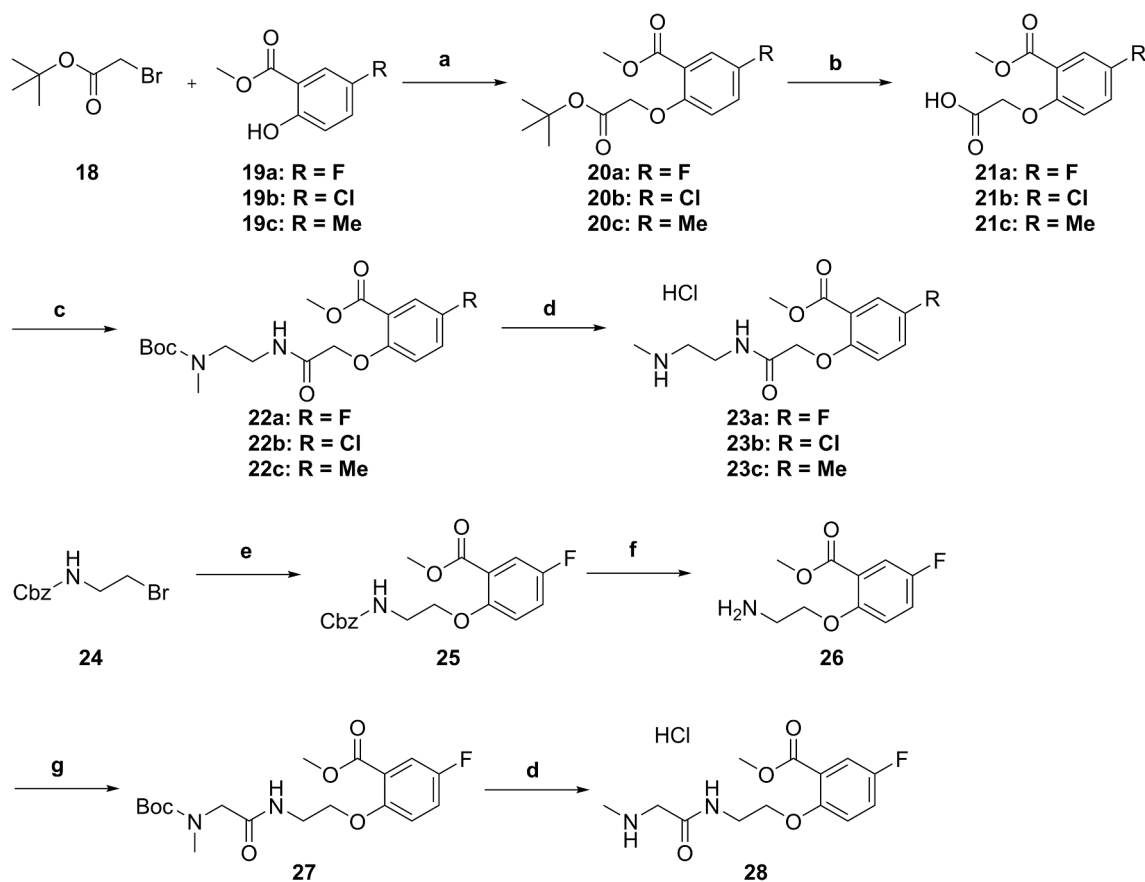


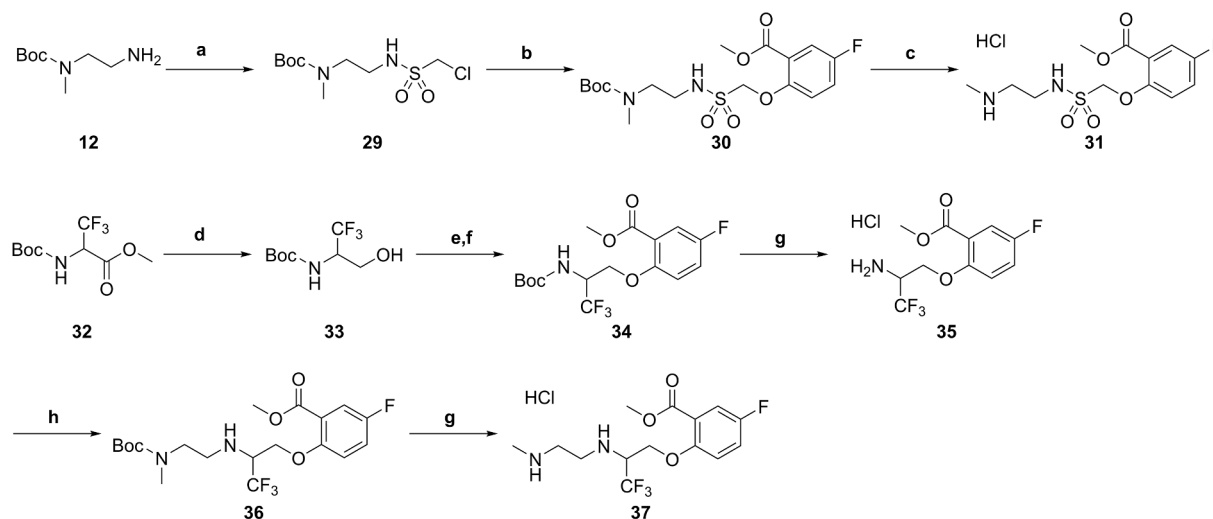
Fig. 1. Chemical structures of RSV F protein inhibitors investigated during early clinical and preclinical studies.



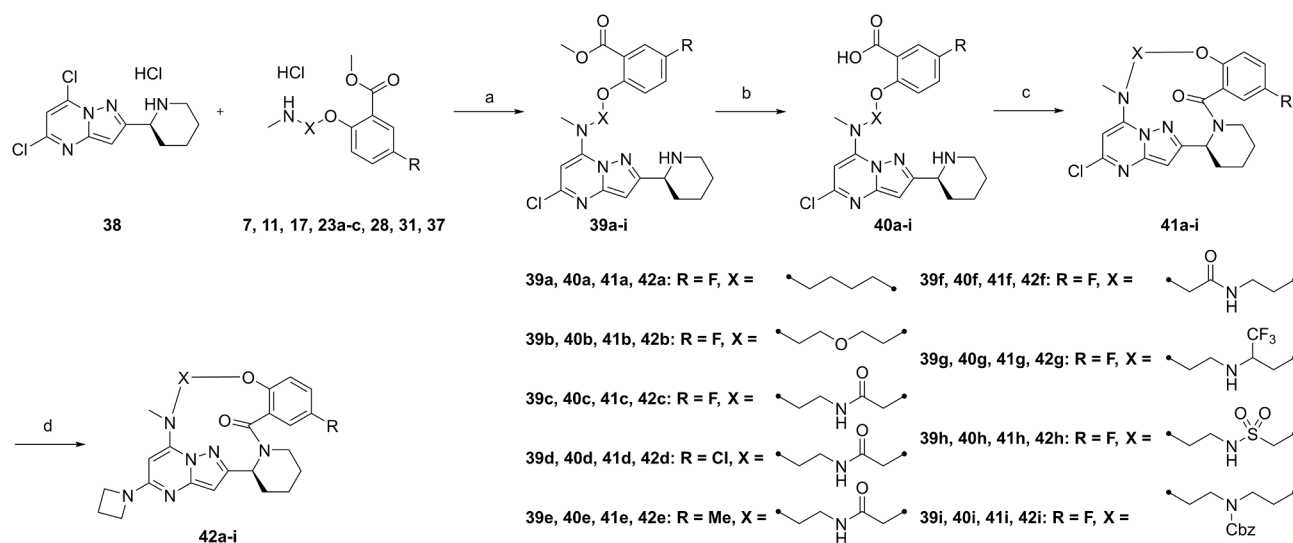
Scheme 1. Synthesis of linker parts. Reagents and conditions: (a) MsCl, Et₃N, CHCl₃, r.t., (b) methyl 5-fluoro-2-hydroxybenzoate, K₂CO₃, DMF, 90 °C, (c) 4M HCl in dioxane, 1,4-dioxane, r.t. (d) MeI, Ag₂O, DMF, 90 °C, (e) 2-bromoethoxy-*tert*-butyldimethylsilane, K₂CO₃, MeCN, 80 °C, (f) benzyl chloroformate, Et₃N, CHCl₃, r.t. (g) TBAF, THF, r.t.



Scheme 2. Synthesis of amide-type linker parts. Reagents and conditions: (a) K₂CO₃, MeCN, 70 °C, (b) TFA, CHCl₃, r.t. (c) *tert*-butyl *N*-(2-aminoethyl)-*N*-methylcarbamate, HATU, Et₃N, DMF, r.t., (d) 4M HCl in dioxane, 1,4-dioxane, r.t. (e) methyl 5-fluoro-2-hydroxybenzoate, NaH, THF, reflux, (f) H₂, Pd/C, MeOH, r.t., (g) 2-[*tert*-butoxycarbonyl(methyl)amino]acetic acid, HATU, Et₃N, DMF, r.t.,



Scheme 3. Synthesis of linker parts with amide isosteres. Reagents and conditions: (a) chloromethanesulfonyl chloride, Et₃N, CHCl₃, 0 °C, (b) methyl 5-fluoro-2-hydroxybenzoate, K₂CO₃, DMF, 80 °C, (c) 4M HCl in dioxane, 1,4-dioxane, r.t. (d) LiBH₄, THF, r.t., (e) MsCl, Et₃N, CHCl₃, r.t., (f) methyl 5-fluoro-2-hydroxybenzoate, K₂CO₃, DMF, 90 °C, (g) 4M HCl in dioxane, 1,4-dioxane, r.t. (h) *tert*-butyl *N*-methyl-*N*-(2-oxoethyl)carbamate, NaHB(OAc)₃, CHCl₃, r.t.



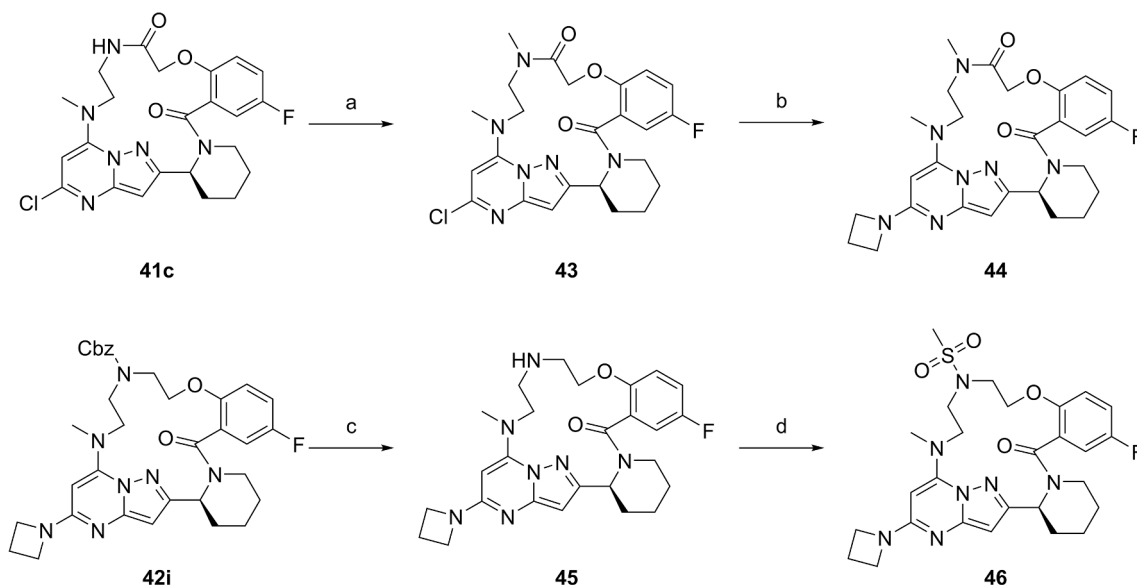
Scheme 4. Synthesis of macrocyclic derivatives. Reagents and conditions: (a) Et₃N, EtOH, 70 °C, (b) 1M NaOH aq., THF, 2-propanol, 80 °C. (c) HATU, Et₃N, DMF, r.t. (d) azetidine, Et₃N, NMP, microwave 150 °C

Furthermore, the macrocyclic products **44**, **45**, and **46** were synthesized as shown in **Scheme 5** using the intermediates **41c** and **42i**. Compound **44** was synthesized by methylation of the amide moiety of **41c** and the introduction of an azetidine at the 5-position of the pyrazolo[1,5-*a*]pyrimidine scaffold. Compound **45** was prepared from **42i** by deprotecting the Cbz group, followed by mesylation of the resulting amine to obtain **46**.

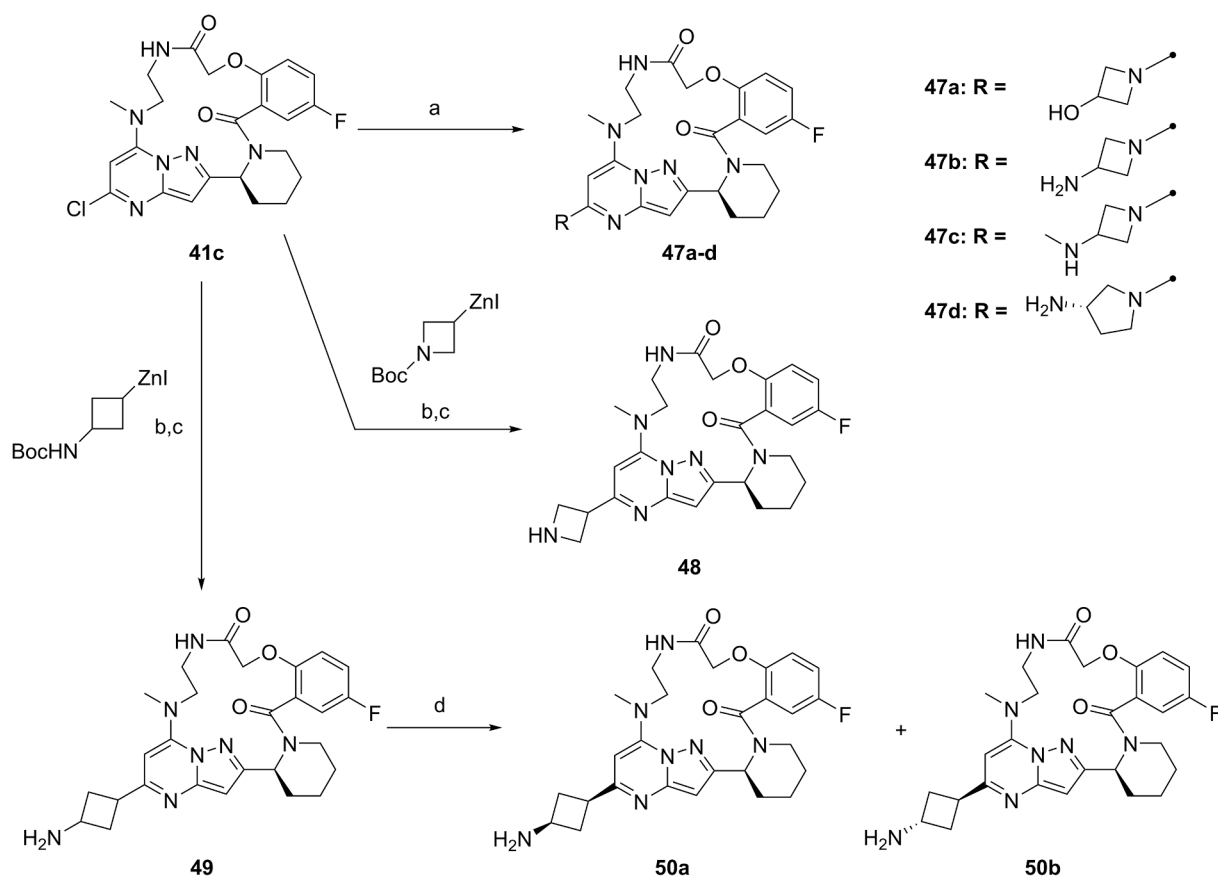
Scheme 6 shows the synthesis of macrocyclic derivatives with modified C-5 substituents of the pyrazolo[1,5-*a*]pyrimidine scaffold. The desired macrocyclic products **47a-d** were synthesized from the intermediate **41c** by introducing appropriate amine parts under microwave irradiation and basic conditions and deprotecting the Boc group, as needed. Compound **48** was synthesized from the intermediate **41c** using the Negishi coupling reaction with an organic zinc reagent, followed by deprotection of the Boc group. The racemic mixture **49**, which was synthesized in the same manner as **48**, was separated using a chiral column to obtain *cis*-isomer **50a** and *trans*-isomer **50b**.

Scheme 7 shows the synthesis of macrocyclic derivatives in which the 3-hydroxycyclobutyl group was introduced into the 5-position of the

pyrazolo[1,5-*a*]pyrimidine scaffold. 3-Benzyloxycyclobutanecarboxylic acid **51** and potassium 3-ethoxy-3-oxopropanoate were treated with 1,1'-carbonyldiimidazole in the presence of magnesium chloride to obtain a ketoester **52**. An aminopyrazole derivative **53**, which was prepared as described in our previous paper,⁴⁵ was reacted with **52** in acetic acid, followed by Boc protection of the amino group to obtain an intermediate **54**. After the chlorination of **54** with phosphorus oxychloride and 4-(*N,N*-dimethylamino)pyridine (DMAP) in pyridine, the resulting *cis/trans* mixture was separated using silica gel column chromatography to obtain **55a,b**. The *cis*-intermediate **55a** was obtained preferentially from **54** over the *trans*-intermediate **55b**. Rather than synthesizing *cis*-isomers **59a-c** and *trans*-isomers **60a-c** from their corresponding intermediates, respectively, it took a few steps to synthesize **59a-c** and **60a-c** by a single reaction route with Mitsunobu inversion. The *cis*-isomer **55a** was aminated with linker parts **23a-c**, followed by hydrolyzation and deprotection of the Boc group, then subjected to intramolecular condensation under a high-dilution condition to yield macrocyclic compounds **58a-c**. Finally, the desired *cis*-isomers **59a-c** were synthesized by removing the benzyl group of **58a-c**. The desired



Scheme 5. Synthesis of macrocyclic derivatives. Reagents and conditions: (a) NaH, MeI, DMF, r.t. (b) azetidine, Et₃N, NMP, microwave 150 °C, (c) H₂, Pd/C, MeOH, r.t., (d) MsCl, Et₃N, CHCl₃, r.t.



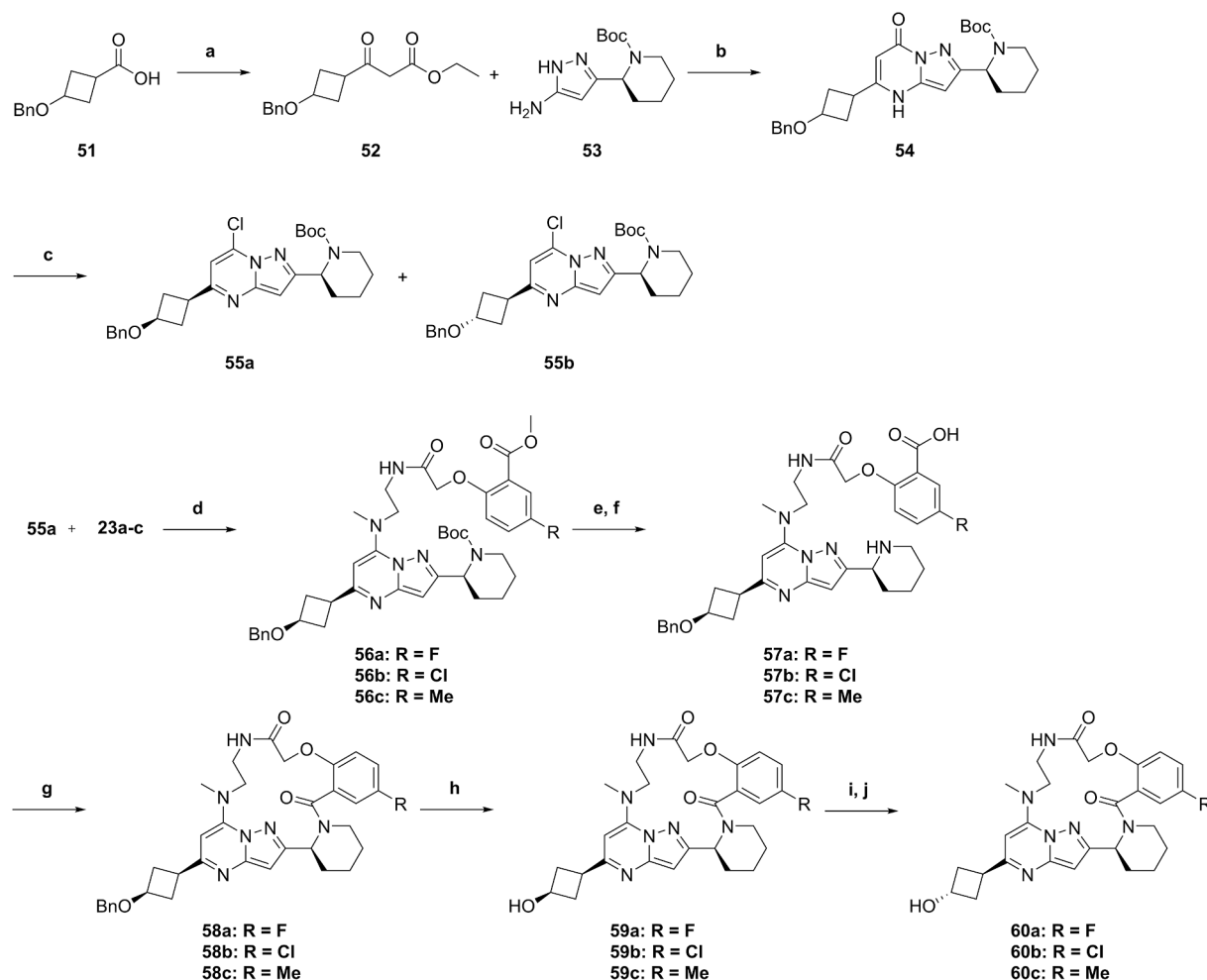
Scheme 6. Synthesis of pyrazolo[1,5-a]pyrimidin-2-yl derivatives with modified C-5 substituents. Reagents and conditions: (a) amine, Et₃N, NMP, microwave 150 °C, then TFA, CHCl₃, r.t. (only for compounds possessing Boc group), (b) CuI, PdCl₂(dppf), DMA, 85 °C, (c) TFA, CHCl₃, r.t. (d) chiral column separation

trans-isomers **60a–c** were synthesized from *cis*-isomers **59a–c** through a Mitsunobu inversion reaction.

3. Results and discussion

The interconversion rates of individual atropisomers of a compound

with a 15-membered ring were determined using NMR spectra at the temperature range from room temperature (25 °C) to 90 °C. Because lead compound **4** was unstable under high-temperature conditions, its analogue **42a** was used for the NMR experiments. Two-dimensional exchange spectroscopy (EXSY) is an effective approach for studying dynamic processes using NMR. The EXSY spectra of **42a** showed no



Scheme 7. Synthesis of pyrazolo[1,5-a]pyrimidin-2-yl derivatives with modified C-5 substituents. Reagents and conditions: (a) potassium 3-ethoxy-3-oxopropionate, CDI, MgCl₂, THF, 65 °C, (b) AcOH, 100 °C, then, Boc₂O, Et₃N, CHCl₃, r.t., (c) POCl₃, DMAP, pyridine, 65 °C, (d) Et₃N, DMF, 80 °C, (e) 1M NaOH aq., THF, MeOH, 60 °C, (f) 4M HCl in 1,4-dioxane, 1,4-dioxane, r.t., (g) HATU, Et₃N, DMF [0.02 M], r.t., (h) TMSCl, NaI, MeCN, 65 °C, (i) *p*-nitrobenzoic acid, bis(2-methoxyethyl)azodicarboxylate, PPh₃, THF, 60 °C, (j) 1M NaOH aq., THF, r.t.

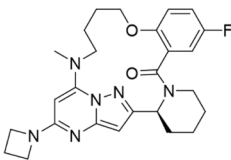
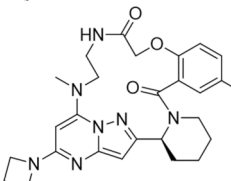
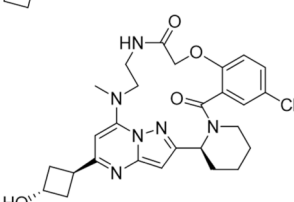
exchange in signals at 25 °C; however, exchange signals were observed at 80 °C. The interconversion rate and the rotation half-life of **42a** at each temperature were calculated from the ratios of the EXSY signal intensities, and the rotation half-life at 25 °C was extrapolated from the interconversion rates at 60 °C, 70 °C, 80 °C, and 90 °C. As a result, the rotation half-life of **42a** for interconversion between two atropisomers was determined to be about 5 min at 25 °C, which was consistent with a class 2 atropisomer (Table 1). Increasing the macrocyclic ring size of the 15-membered macrocyclic compound **42a** seemed a plausible strategy for changing the class 2 compound to class 1 compounds with smaller rotation barriers, which would have appropriate developability profiles. This process was expected to improve the rotation rate by decreasing the rotation barrier of **42a** due to the tightness of the ring. Our previous studies indicated that compounds with a 16-membered ring maintained potent anti-RSV activity, while the activity of compounds with a 17-membered ring was greatly reduced.⁴¹ Therefore, the optimization study of macrocyclic compounds was mainly focused on 16-membered ring.

The inhibition of the cytopathic effect (CPE) induced by RSV infection was used to evaluate the antiviral activities of the synthesized compounds. Table 2 shows the anti-RSV A2 activities of **4** and macrocyclic compounds (**42a–c**, **42f–h**, **44–46**) with a modified linker moiety connecting the 2-position of the benzoyl moiety and the 7-position of the pyrazolo[1,5-a]pyrimidine scaffold. The previous studies only showed the SAR of compounds with a hydrocarbon linker moiety; therefore, the

effect of the incorporation of a polar group into the linker moiety was investigated in this study with the expectation of obtaining an additional interaction as a proton donor or a proton acceptor. The introduction of an oxygen atom into the linker moiety of **42a** (EC₅₀: 17 nM) produced no change in anti-RSV activity (**42b**, EC₅₀: 17 nM). Compound **45** containing a nitrogen atom in the linker moiety exhibited an improved anti-RSV activity (EC₅₀: 1.4 nM) by more than 10-fold, compared with **42a**. Furthermore, **42c** possessing an amide group in the linker moiety had a highly potent anti-RSV activity (EC₅₀: 0.33 nM), which led us to investigate the activity of analogues of **42c** containing an amide linker. The *N*-methylation of the amide group (**44**) and the change in the position of the carbonyl group (**42f**) reduced the anti-RSV activities by 4.2- and 7.6-fold [EC₅₀: 1.4 nM (**44**), 2.5 nM (**42f**)] compared with **42c**, respectively. The introduction of trifluoroethylamine as an amide isostere markedly reduced the anti-RSV activity (**42 g**, EC₅₀: 21 nM). In addition, the anti-RSV activities of **46** and **42 h** with a sulfonamide group were markedly attenuated compared with **42c** [EC₅₀: 4.6 nM (**46**), 54 nM (**42 h**)]. Among the compounds containing a 16-membered ring with a variety of linker structures, compound **42c** exhibited the most potent anti-RSV activity, exceeding that of **4** with a 15-membered ring [EC₅₀: 2.0 nM (**4**)].⁴¹

To investigate the effect of ring expansion on the rate of atropisomer interconversion, an EXSY analysis of **42c** was performed. Compound **42c** showed a clear exchange of signals at 25 °C; the rotation half-life of **42c** for interconversion between two atropisomers was determined to be

Table 1
Structures and rotation half-lives of representative pyrazolo[1,5-*a*]pyrimidine derivatives.

Compound	Structure	Ring size	Rotation $t_{1/2}$ (DMSO- d_6 , 25 °C)		Atropisomer classification
			main	minor	
42a		15	4.92 min ^a	6.30 min ^a	Class 2
42c		16	1.90 s	2.21 s	Class 1
60b		16	2.31 s	2.35 s	Class 1

^a The rotation half-lives were extrapolated from the interconversion rates at high temperatures.

about 2 s, indicating that **42c** was classified as a class 1 non-atropisomer (Table 1).

As expected, increasing the macrocyclic ring size proved to be an effective strategy for changing a class 2 compound (**42a**, 15-membered ring) into a class 1 compound (**42c**, 16-membered ring).

To further enhance the anti-RSV activity, our subsequent SAR study was focused on optimizing the 5-position (R_1) of the pyrazolo[1,5-*a*]pyrimidine scaffold of **42c**. Table 3 shows the anti-RSV A2 activity of **42c** derivatives with 5-position substituents. Previous SAR studies of a variety of pyrazolo[1,5-*a*]pyrimidine derivatives revealed that a basic group such as aminopyrrolidine at the 5-position improved the anti-RSV A2 activity because of the formation of a hydrogen bond between the basic group and the Asp⁴⁸⁶ residue in the F protein. These findings have been applied to a study of a series of non-macrocyclic derivatives^{45,46} and macrocyclic derivatives such as **4** with a hydrocarbon linker,⁴¹ which motivated us to introduce mainly basic functional groups into the 5-position of the pyrazolo[1,5-*a*]pyrimidine scaffold. Compound **47a** with a hydroxyl group at the 3-position of an azetidine ring exhibited a potent anti-RSV activity comparable to that of **42c** [EC₅₀: 0.33 nM (**42c**), 0.81 nM (**47a**)], whereas **47b** and **47c** with an amino group and a methylamino group, respectively, showed attenuated activities [EC₅₀: 2.7 nM (**47b**), 7.0 nM (**47c**)]. The substitution of the 3-aminoazetidin-1-yl group of **47b** with a (3*S*)-3-aminopyrrolidin-1-yl group (**47d**), i.e., ring expansion, slightly improved the activity (**47d**, EC₅₀: 2.1 nM). A regioisomer (**48**) of **42c**, in which the azetidine ring was reversed, showed a decreased activity by 5.2-fold (**48**, EC₅₀: 1.7 nM). Unlike the previously reported SAR as mentioned above,^{41,45,46} the anti-RSV A2 activity of the derivatives with an amide linker was not improved by the introduction of basic groups. Among compounds containing a basic group at the 5-position of the pyrazolo[1,5-*a*]pyrimidine scaffold, **50a** (*cis*-isomer) and **50b** (*trans*-isomer) possessing a 3-aminocyclobutyl group showed the highest potency, with EC₅₀ values around 1 nM [EC₅₀: 0.87 nM (**50a**), 1.1 nM (**50b**)]. The replacement of the amino groups of **50a** and **50b** with hydroxyl groups [**59a** (*cis*-isomer) and **60a** (*trans*-isomer)] did not affect the anti-RSV activity [EC₅₀: 1.1 nM (**59**), 0.74 nM (**60a**)]. In each case, there was no significant difference in the anti-RSV activity between the *cis* and *trans* isomers. A series of compounds with basic functional groups at the 5-position of the pyrazolo

[1,5-*a*]pyrimidine scaffold, such as **47b**, **47d**, **48**, **50a**, and **50b**, showed potent activities; however, all of these compounds had relatively low membrane permeabilities in a parallel artificial membrane permeability assay (PAMPA), suggesting that the introduction of a basic group was not preferable for oral administration.

To obtain orally available anti-RSV inhibitors, a subsequent optimization study on substituents (R_2) of the aryl moiety was performed using **42c** and **60a** as lead compounds with potent anti-RSV A2 activities and good membrane permeabilities (Table 4). Previous studies have shown that compounds with a chlorine atom or a methyl group at R_2 also possessed good anti-RSV activities.⁴⁵ However, no improvement of activity was observed when replacing the fluorine atom by a chlorine atom (**42d**) or a methyl group (**42e**) on the benzene ring of **42c** with an azetidine moiety [EC₅₀: 0.33 nM (**42c**), 0.47 nM (**42d**), 0.64 nM (**42e**)]. Conversely, in the case of the derivatives of **60a** with a 3-hydroxycyclobutyl moiety, the replacement of the fluorine atom by a chlorine atom (**60b**) at the 5-position of the benzene ring of **60a** showed improved anti-RSV activity, compared with that of **60a** [EC₅₀ values: 0.74 nM (**60a**), 0.27 nM (**60b**)]. The anti-RSV activity of **60c** with a methyl group as an R_2 substituent was found to be comparable to that of **60a** [EC₅₀ value: 0.77 nM (**60c**)]. The in vitro ADMET studies of **42c**, **42d**, **42e**, **60a**, **60b**, and **60c** showed that **42e** and **60c** containing a methyl group at the 5-position of the benzene ring had a relatively strong CYP3A metabolism-dependent inhibition (MDI). Compounds **42c** and **60b**, which showed more potent anti-RSV activities against A2 than other compounds, also exhibited potent activities against the clinically isolated D486N mutant, with EC₅₀ values of 3.1 nM and 0.70 nM, respectively. The EC₅₀ value of **60b** was in the sub-nanomolar range, and the difference in the EC₅₀ values of activities against A2 and the D486N mutant was only 2.6-fold. Compound **60b** exhibited preferred protein binding in human and mouse plasma. To investigate the rate of atropisomer interconversion, an EXSY analysis of **60b** was performed. Compound **60b** showed clear signals at 25 °C; the rotation half-life of **60b** for interconversion between two atropisomers was determined to be about 2 s, indicating that **60b** was also classified as a class 1 non-atropisomer (Table 1).

Fig. 2 shows the binding model of compound **60b** with the crystallographic structure of RSV A2 F protein (Protein Data Bank entry 5EA3).

Table 2
Structures and antiviral activities of pyrazolo[1,5-*a*]pyrimidine derivatives with a series of linkers.

Compound	Structure	Anti-RSV activity
		EC ₅₀ (nM) ^a A2
4		2.0
42a		17
42b		17
42c		0.33
42f		2.5
42g		21
42h		54
44		1.4
45		1.4
46		4.6

Table 2 (continued)

Compound	Structure	Anti-RSV activity
		EC ₅₀ (nM) ^a A2

^a EC₅₀ values of the CPE inhibitory activities of all the compounds were evaluated in HEP-2 cells infected with RSV A2.

Three characteristic interactions are seen in the interface of **60b** and A2: (1) the pyrazolo[1,5-*a*]pyrimidine ring is sandwiched between two Phe⁴⁸⁸ residues of the F protein trimer to form π - π interactions; (2) the 3-hydroxycyclobutyl group forms hydrogen bonds with the carboxyl group of Asp⁴⁸⁶; and (3) an intramolecular hydrogen bond is formed between the amide linker moiety and the nitrogen atom at the 1-position of the pyrazolo[1,5-*a*]pyrimidine scaffold. The intramolecular hydrogen bond is a new interaction that was not observed in the previous compounds with a hydrocarbon linker, such as **4**.⁴¹ Therefore, the intramolecular hydrogen bond of **60b** appears to be a critical factor in the highly potent anti-RSV activities against both A2 and the D486N mutant by enabling suitable conformations of **60b** on the surface of both proteins.

Table 3

Structures and antiviral activities of pyrazolo[1,5-*a*]pyrimidine derivatives with a substituent R₁.

Compound	R ₁	Anti-RSV activity EC ₅₀ (nM) ^a A2	PAMPA pH 6.2 (10 ⁻⁶ cm/s)
42c		0.33	80
47a		0.81	8.0
47b		2.7	3.3
47c		7.0	5.9
47d		2.1	0.3
48		1.7	0
50a		0.87	0
50b		1.1	0
59a		1.1	28
60a		0.74	27

^a EC₅₀ values of the CPE inhibitory activities of all the compounds were evaluated in HEP-2 cells infected with RSV A2.

Table 4Structures and antiviral activities of pyrazolo[1,5-*a*]pyrimidine derivatives with substituents R₁ and R₂.

Compound	R ₁	R ₂	EC ₅₀ (nM) ^a A2	EC ₅₀ (nM) ^a D486N	CYP3A MDI (%) @10 μM	Protein binding (human/ mouse) (%)
42c		F	0.33	3.1	-4.7	87.0/98.0
42d		Cl	0.47	NT	-2.9	NT
42e		Me	0.64	NT	60.1	93.6/96.9
60a		F	0.74	NT	0.4	NT
60b		Cl	0.27	0.70	-1.4	90.7/85.5
60c		Me	0.77	NT	57.0	88.8/77.8

^a EC₅₀ values of the CPE inhibitory activities of all the compounds were evaluated in HEP-2 cells infected with RSV A2 or D486N.

4. Conclusion

The present NMR studies clarified the presence of atropisomers of the 15-membered macrocyclic compound **42a** with a rotation half-life of about 5 min at 25 °C, consistent with a class 2 atropisomer with a very low developability profile. To improve the developability profile of the subsequent series of compounds, we investigated the possibility of using

ring size expansion along with linker structure optimization. These efforts led to the discovery of a class 1 compound **42c** with a 16-membered ring with an amide moiety, which showed an atropisomer rotation half-life of about 2 s at 25 °C. Among compounds with different linker structures, **42c** showed the most potent anti-RSV activity against the A2. The molecular dynamics studies of **42c** suggested that the amide linker forms an intramolecular hydrogen bond with the pyrazolo[1,5-*a*]pyrimidine scaffold. This intramolecular hydrogen bond appears to contribute to the enhanced anti-RSV activity. Subsequent optimization of the R₁ and R₂ groups of the pyrazolo[1,5-*a*]pyrimidine and benzene ring, respectively, led to the discovery of a promising macrocyclic compound **60b**, which showed potent anti-RSV activities against both the wild-type and D486N mutant F proteins. Compound **60b** has been selected as a clinical candidate, and further detailed evaluations of its therapeutic potential are underway.

5. Experimental section

5.1. Chemistry

All solvents and reagents were purchased from commercial suppliers and used without purification or were prepared according to published procedures. The ¹H NMR and ¹³C NMR spectra of compounds synthesized in this study were recorded using a JNM-ECA600, JNM-ECA500 (JEOL Ltd., Tokyo, Japan), or Avance III HD 400 (Bruker Corp., Billerica, MA, USA), and the chemical shifts were expressed in δ (:) values, with tetramethylsilane as the internal standard (s = singlet, d = doublet, t = triplet, q = quartet, m = multiplet, and brs = broad singlet). Two sets of NMR signals were observed because of structural variations of the *cis*- and *trans*-amide rotamers. Mass spectra were recorded on a Micromass Platform LC (Micromass Ltd., Manchester, UK) or Shimadzu LCMS-2010EV (Shimadzu Corp., Kyoto, Japan). High-resolution (HR) mass spectral data were acquired using an LCMS-IT-TOF equipped with an electrospray ionization (ESI)/atmospheric pressure chemical ionization (APCI) dual ion source (Shimadzu Corp.). Intermediates and final compounds were purified using preparative HPLC and an Agilent 1260 Infinity/Agilent 6130 (Agilent Technologies Inc., Santa Clara, CA, USA) or a GX-281, UV/VIS-155, 331 PUMP, 332 PUMP, or SOFTA Model 300S

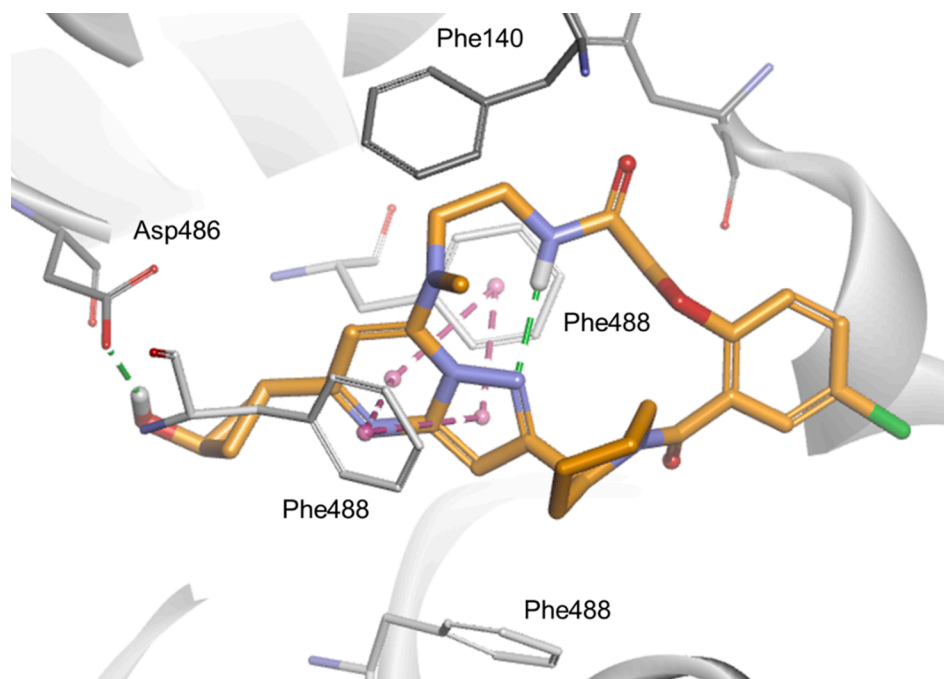


Fig. 2. Molecular dynamics model of **60b** binding to the RSV A2 F protein. Molecular dynamics model showing **60b** (orange) binding to the RSV A2 F protein (gray). The hydrogen bonds are depicted as a dashed light green line. The π - π interactions are depicted as dashed pink lines.

ELSD (Gilson Inc., Middleton, WI, USA) under the following conditions: column, Sunfire prep C18 OBD (5.0 μ m, 30 mm \times 50 mm) (Waters Corp., Milford, MA, USA), YMC-Actus Triart C18 (5.0 μ m, 30 mm \times 50 mm) (YMC Co., Ltd., Kyoto, Japan), Xbridge Prep C18 OBD (5.0 μ m, 30 mm \times 50 mm) (Waters Corp.), or XSelect CSH C18 (5.0 μ m, 30 mm \times 50 mm) (Waters Corp.); flow, 50 mL/min; linear gradient, 10%–95% acetonitrile in water containing 0.1% formic acid for 7.5–11.5 min; detection wavelength, 254 nm. The purity of the synthesized compounds was determined using an LC-MS system (Agilent 1290 Infinity, Agilent Technologies Inc.) under the following conditions: column, ACQUITY UPLC CSH C18 (1.7 μ m, 2.1 \times 50 mm) (Waters Corp.); flow, 0.8 mL/min; linear gradient, 20%–99% acetonitrile in water containing 0.1% formic acid in 1.2 min; detection wavelength, 254 nm. All final compounds had a purity of \geq 95%.

5.2. Synthesis of key compounds

5.2.1. Methyl 2-[2-[2-[5-chloro-2-[(2S)-2-piperidyl]pyrazolo[1,5-a]pyrimidin-7-yl]-methyl-amino]ethylamino]-2-oxo-ethoxy]-5-fluorobenzoate (39c)

To a solution of **38** (0.43 g, 1.25 mmol) in ethanol (12 mL) was added **23a** (0.44 g, 1.37 mmol, 1.1 eq) and triethylamine (1.7 mL, 12.5 mmol, 10 eq), and the mixture was stirred at 70 °C for 0.5 h. The reaction mixture was poured into saturated aqueous sodium bicarbonate and extracted with chloroform. The organic layer was washed with brine, dried over magnesium sulfate, filtered, and concentrated under reduced pressure. The residue was purified using silica gel column chromatography (NH 70% ethyl acetate in hexane) to obtain **39c** (0.36 g, 0.694 mmol, 56%) as a colorless amorphous substance.

¹H NMR (400 MHz, CDCl₃) δ ppm 1.46–1.71 (m, 4H), 1.79–1.92 (m, 1H), 1.95–2.03 (m, 1H), 2.75–2.83 (m, 1H), 3.14–3.21 (m, 1H), 3.23 (s, 3H), 3.74 (q, J = 6.07 Hz, 2H), 3.80–3.86 (m, 4H), 4.34 (s, 2H), 4.40 (t, J = 5.99 Hz, 2H), 5.90 (s, 1H), 6.23 (s, 1H), 6.74–6.82 (m, 1H), 7.16–7.24 (m, 1H), 7.54–7.60 (m, 1H), 8.35–8.44 (m, 1H), MS (ESI/APCI dual) m/z : 519 [M + H]⁺

5.2.2. (18aS)-13-Chloro-2-fluoro-11-methyl-8,9,10,11,19,20,21,22-octahydro-18aH,24H-18,15-(metheno)pyrido[2,1-l]pyrimido[6,1-h][1,4,7,9,10,13]benzoxapentaazacyclohexadecine-7,24(6H)-dione (41c)

To a solution of **39c** (0.36 mg, 0.694 mmol) in THF (7.0 mL) and 2-propanol (7.0 mL) was added 1 M aqueous sodium hydroxide (14 mL, 13.9 mmol, 20 eq), and the mixture was stirred at 80 °C for 0.5 h. The reaction mixture was acidified with 1 M aqueous hydrochloric acid and extracted with chloroform. The organic layer was dried through a phase separator and concentrated under reduced pressure to obtain 2-[2-[2-[5-chloro-2-[(2S)-2-piperidyl]pyrazolo[1,5-a]pyrimidin-7-yl]-methyl-amino]ethylamino]-2-oxo-ethoxy]-5-fluorobenzoic acid (**40c**) (0.40 g, 0.792 mmol, quant.) as a colorless amorphous substance. This compound was used in the next reaction without further purification.

To a solution of **40c** (0.40 g, 0.792 mmol) in *N,N*-dimethylformamide (79 mL, 0.01 M) was added triethylamine (0.55 mL, 3.96 mmol, 5.0 eq) and 1-[bis(dimethylamino)methylene]-1H-1,2,3-triazolo[4,5-b]pyridinium 3-oxide hexafluorophosphate (0.45 g, 1.19 mmol, 1.5 eq). After stirring at room temperature for 15 h, the reaction mixture was poured into saturated aqueous sodium bicarbonate and extracted with ethyl acetate/toluene (1:1). The organic layer was washed with brine, dried over magnesium sulfate, filtered, and concentrated under reduced pressure. The residue was purified using silica gel column chromatography (OH 85% ethyl acetate in hexane to 7% methanol in chloroform) to obtain **41c** (0.25 g, 0.518 mmol, 65%) as a yellow amorphous substance.

¹H NMR (400 MHz, CDCl₃) δ ppm 1.41–2.21 (m, 5H), 2.31–2.42 (m, 0.4H), 2.85–2.99 (m, 0.6H), 3.01–3.33 (m, 6.3H), 4.21–4.58 (m, 3.1H), 4.75–4.85 (m, 0.6H), 4.97–5.03 (m, 0.6H), 5.03–5.15 (m, 0.4H), 5.16–5.28 (m, 0.6H), 6.06 (s, 0.6H), 6.11 (s, 0.4H), 6.21 (s, 0.6H), 6.30–6.37 (m, 0.4H), 6.56 (s, 0.4H), 6.80–6.89 (m, 1H), 6.98–7.11 (m,

2H), 7.65–7.78 (m, 0.4H), 8.69–8.81 (m, 0.6H), ¹³C NMR (151 MHz, DMSO-*d*₆) δ ppm 19.7, 24.7, 29.8, 36.3, 37.3, 43.5, 46.9, 48.9, 54.0, 70.6, 79.1, 91.0, 113.8, 116.4, 119.3, 130.1, 149.5, 150.2, 150.3, 150.8, 155.2, 165.6, 167.3, MS (ESI/APCI dual) m/z : 487 [M + H]⁺

5.2.3. (18aS)-13-(Azetidin-1-yl)-2-fluoro-11-methyl-8,9,10,11,19,20,21,22-octahydro-18aH,24H-18,15-(metheno)pyrido[2,1-l]pyrimido[6,1-h][1,4,7,9,10,13]benzoxapentaazacyclohexadecine-7,24(6H)-dione (42c)

To a solution of **41c** (0.10 g, 0.205 mmol) in 1-methyl-2-pyrrolidone (1.5 mL) was added triethylamine (0.57 mL, 4.11 mmol, 20 eq) and azetidine (0.14 mL, 2.05 mmol, 10 eq). After stirring at 150 °C under microwave irradiation for 30 min, the reaction mixture was purified using reverse-phase preparative HPLC to obtain **42c** (53 mg, 0.104 mmol, 51%) as a colorless powder.

¹H NMR (600 MHz, DMSO-*d*₆) δ ppm 1.39–1.77 (m, 4H), 1.81–1.98 (m, 1H), 2.05–2.12 (m, 0.7H), 2.15–2.21 (m, 0.3H), 2.26–2.35 (m, 2H), 2.83 (s, 0.9H), 2.89 (s, 2.1H), 2.97–3.20 (m, 2.7H), 3.35–3.42 (m, 0.3H), 3.80–3.89 (m, 0.3H), 3.93–4.10 (m, 6H), 4.47–4.55 (m, 1.7H), 4.63–4.76 (m, 1.7H), 5.30 (s, 0.7H), 5.37 (m, 0.3H), 5.87 (s, 0.7H), 5.96–6.00 (m, 0.3H), 6.08 (s, 0.3H), 7.09–7.15 (m, 0.7H), 7.15–7.28 (m, 1.6H), 7.30–7.37 (m, 0.7H), 7.48–7.57 (m, 0.3H), 8.97 (d, J = 6.61 Hz, 0.7H)

¹³C NMR (151 MHz, DMSO-*d*₆) δ ppm 15.6, 19.8, 24.7, 29.5, 36.4, 37.9, 43.6, 46.9, 48.3, 50.1, 54.0, 71.2, 78.0, 89.4, 113.7, 116.5, 120.0, 130.7, 149.6, 150.3, 151.6, 153.4, 156.9, 158.5, 165.4, 167.5; HRMS ESI/APCI dual m/z calcd for C₂₆H₃₀N₇O₃ [M + H]⁺ 508.2467, found 508.2444

5.2.4. Ethyl 3-(3-benzyloxycyclobutyl)-3-oxo-propanoate (52)

To a solution of 3-benzyloxycyclobutanecarboxylic acid (5.3 g, 26 mmol) in THF (86 mL) was added 1,1'-carbonyldiimidazole (6.3 g, 39 mmol, 1.5 eq). After stirring at room temperature for 2.5 h, the reaction mixture was added to potassium 3-ethoxy-3-oxo-propanoate (8.7 g, 51 mmol, 2.0 eq) and magnesium chloride (4.9 g, 51 mmol, 2.0 eq). After stirring at 65 °C for 2.5 h, the reaction mixture was cooled to room temperature and filtered through a pad of Celite®, and the filtrate was concentrated under reduced pressure. The residue was purified using silica gel column chromatography (OH 5%–20% ethyl acetate in hexane) to obtain **52** (3.1 g, 11.5 mmol, 45%) as a colorless oil.

¹H NMR (400 MHz, CDCl₃) δ ppm 1.23–1.32 (m, 3H), 2.14–2.34 (m, 2H), 2.39–2.59 (m, 2H), 2.82–2.95 (m, 1H), 3.38–3.45 (m, 2H), 3.93–4.05 (m, 1H), 4.13–4.24 (m, 2H), 4.37–4.47 (m, 2H), 7.27–7.37 (m, 5H), MS (ESI/APCI dual) m/z : 277 [M + H]⁺

5.2.5. tert-Butyl (2S)-2-[5-(3-benzyloxycyclobutyl)-7-oxo-4H-pyrazolo[1,5-a]pyrimidin-2-yl]piperidine-1-carboxylate (54)

To a solution of **52** (3.1 g, 11 mmol, 1.2 eq) in acetic acid (23 mL) was added *tert*-butyl (2S)-2-(5-amino-1H-pyrazol-3-yl)piperidine-1-carboxylate (2.5 g, 9.4 mmol). After stirring at 100 °C for 2.5 h, the reaction mixture was cooled to room temperature and was concentrated under reduced pressure. To a solution of the resulting residue in chloroform (31 mL) was added triethylamine (2.6 mL, 19 mmol, 2.0 eq) and di-*tert*-butyl dicarbonate (2.0 g, 9.4 mmol, 1.0 eq). After stirring for 2 h at room temperature, the reaction mixture was poured into 0.5 M aqueous hydrochloric acid and extracted with chloroform. The organic layer was dried through a phase separator and concentrated under reduced pressure. The residue was purified using silica gel column chromatography (OH 50%–100% ethyl acetate in hexane) to obtain **54** (4.0 g, 8.3 mmol, 88%) as a colorless amorphous substance.

¹H NMR (400 MHz, CDCl₃) δ ppm 1.31–1.80 (m, 13H), 2.12–2.26 (m, 2H), 2.42–2.56 (m, 0.8H), 2.57–2.88 (m, 3.4H), 3.01–3.17 (m, 0.8H), 3.45–3.59 (m, 0.2H), 3.89–4.30 (m, 2.8H), 4.39–4.52 (m, 2H), 5.34–5.46 (m, 1H), 5.51 (s, 0.8H), 5.60–5.81 (m, 1.2H), 7.28–7.43 (m, 5H), 10.51–11.37 (m, 1H), MS (ESI/APCI dual) m/z : 479 [M + H]⁺

5.2.6. *tert*-Butyl (2*S*)-2-{5-[(1*S*,3*R*)-3-(benzyloxy)cyclobutyl]-7-chloropyrazolo[1,5-*a*]pyrimidin-2-yl}piperidine-1-carboxylate (**55a**) and *tert*-butyl (2*S*)-2-{5-[(1*r*,3*S*)-3-(benzyloxy)cyclobutyl]-7-chloropyrazolo[1,5-*a*]pyrimidin-2-yl}piperidine-1-carboxylate (**55b**)

A solution of 4-dimethylaminopyridine (1.8 g, 15.0 mmol, 1.1 eq) in pyridine (68 mL) was cooled to 0 °C, and phosphorus oxychloride (8.7 mL, 95.5 mmol, 7.0 eq) and **54** (6.5 g, 13.6 mmol) were added. After stirring at 65 °C for 0.5 h, the reaction mixture was cooled to room temperature and concentrated under reduced pressure. The residue was purified using silica gel column chromatography (OH ethyl acetate) and (OH 15% ethyl acetate in hexane) to obtain **55a** (3.8 g, 7.76 mmol, 65%) as a pale yellow oil and **55b** (0.90 g, 1.80 mmol, 15%) as a pale yellow oil.

55a: ¹H NMR (400 MHz, CDCl₃) δ ppm 1.37–1.71 (m, 13H), 1.82–1.96 (m, 1H), 2.34 (q, *J* = 9.01 Hz, 2H), 2.50 (d, *J* = 13.20 Hz, 1H), 2.66–2.76 (m, 2H), 2.91 (t, *J* = 11.80 Hz, 1H), 3.07–3.20 (m, 1H), 4.02–4.18 (m, 2H), 4.49 (s, 2H), 5.62 (brs, 1H), 6.49 (s, 1H), 6.80 (s, 1H), 7.27–7.40 (m, 5H), ¹³C NMR (151 MHz, DMSO-*d*₆) δ ppm 19.3, 24.7, 27.8, 28.0, 31.8, 35.7, 35.8, 68.1, 69.0, 78.9, 95.0, 107.3, 127.4, 127.6, 128.1, 137.1, 138.3, 149.7, 154.5, 158.2, 163.3, MS (ESI/APCI dual) *m/z*: 497 [M + H]⁺

55b: ¹H NMR (400 MHz, CDCl₃) δ ppm 1.38–1.71 (m, 13H), 1.81–1.97 (m, 1H), 2.45–2.57 (m, 3H), 2.61–2.72 (m, 2H), 2.85–2.98 (m, 1H), 3.58–3.71 (m, 1H), 4.01–4.17 (m, 1H), 4.32–4.41 (m, 1H), 4.47 (s, 2H), 5.63 (brs, 1H), 6.49 (s, 1H), 6.74 (s, 1H), 7.27–7.39 (m, 5H), ¹³C NMR (151 MHz, DMSO-*d*₆) δ ppm 19.4, 21.7, 27.3, 28.0, 31.0, 33.8, 34.1, 44.2, 53.6, 69.2, 70.8, 79.2, 86.9, 92.2, 127.4, 127.6, 128.2, 138.3, 142.5, 152.5, 154.4, 155.3, 155.9, 156.7, MS (ESI/APCI dual) *m/z*: 497 [M + H]⁺

5.2.7. *tert*-Butyl (2*S*)-2-{5-[(1*S*,3*R*)-3-(benzyloxy)cyclobutyl]-7-[(2-*r*-[4-fluoro-2-(methoxycarbonyl)phenoxy]acetamido)ethyl](methyl)amino]pyrazolo[1,5-*a*]pyrimidin-2-yl}piperidine-1-carboxylate (**56a**)

To a solution of **55a** (0.21 g, 0.425 mmol) in 1-methyl-2-pyrrolidone (4.2 mL) was added triethylamine (0.59 mL, 4.25 mmol, 10 eq) and **23a** (0.19 g, 0.594 mmol, 1.4 eq). After stirring at 150 °C under microwave irradiation for 30 min, the reaction mixture was poured into water and extracted with ethyl acetate. The organic layer was washed with brine and dried over magnesium sulfate, filtered, concentrated under reduced pressure. The residue was purified using silica gel column chromatography (OH 30%–70% ethyl acetate in hexane) to obtain **56a** (0.11 g, 0.145 mmol, 34%) as a colorless amorphous substance.

¹H NMR (400 MHz, CDCl₃) δ ppm 1.36–1.66 (m, 12H), 1.76–1.89 (m, 1H), 2.23–2.34 (m, 2H), 2.35–2.49 (m, 1H), 2.59–2.71 (m, 2H), 2.78–2.91 (m, 1H), 2.94–3.06 (m, 1H), 3.21 (s, 3H), 3.71–3.85 (m, 5H), 3.93–4.28 (m, 5H), 4.47 (s, 4H), 5.53 (brs, 1H), 5.83 (s, 1H), 6.17 (s, 1H), 6.77–6.89 (m, 1H), 7.13–7.22 (m, 1H), 7.28–7.39 (m, 5H), 7.52–7.61 (m, 1H), 8.24–8.36 (m, 1H), MS (ESI/APCI dual) *m/z*: 745 [M + H]⁺

5.2.8. *tert*-Butyl (2*S*)-2-{5-[(1*S*,3*R*)-3-(benzyloxy)cyclobutyl]-7-[(2-*r*-[4-chloro-2-(methoxycarbonyl)phenoxy]acetamido)ethyl](methyl)amino]pyrazolo[1,5-*a*]pyrimidin-2-yl}piperidine-1-carboxylate (**56b**)

To a solution of **55a** (6.7 g, 13.5 mmol) in *N,N*-dimethylformamide (68 mL) was added triethylamine (15.1 mL, 108 mmol, 8.0 eq) and **23b** (6.4 g, 19.0 mmol, 1.4 eq). After stirring at 80 °C for 1 h, the reaction mixture was cooled and was poured into water and extracted with ethyl acetate/toluene (4/1). The organic layer was washed with brine and dried over magnesium sulfate, filtered, and concentrated under reduced pressure. The residue was purified using silica gel column chromatography (OH 25%–100% ethyl acetate in hexane) to obtain **56b** (9.1 g, 11.9 mmol, 88%) as a colorless amorphous substance.

¹H NMR (400 MHz, CDCl₃) δ ppm 1.33–1.69 (m, 12H), 1.75–1.90 (m, 1H), 2.22–2.34 (m, 2H), 2.35–2.49 (m, 1H), 2.60–2.72 (m, 2H), 2.78–2.91 (m, 1H), 2.94–3.07 (m, 1H), 3.20 (s, 3H), 3.70–3.86 (m, 5H), 3.92–4.29 (m, 5H), 4.41–4.55 (m, 4H), 5.53 (brs, 1H), 5.83 (s, 1H), 6.17

(s, 1H), 6.81 (d, *J* = 8.68 Hz, 1H), 7.28–7.46 (m, 6H), 7.83 (s, 1H), 8.22–8.31 (m, 1H), MS (ESI/APCI dual) *m/z*: 761 [M + H]⁺

5.2.9. *tert*-Butyl (2*S*)-2-{5-[(1*S*,3*R*)-3-(benzyloxy)cyclobutyl]-7-[(2-*r*-[2-(methoxycarbonyl)-4-methylphenoxy]acetamido)ethyl](methyl)amino]pyrazolo[1,5-*a*]pyrimidin-2-yl}piperidine-1-carboxylate (**56c**)

According to the procedure described for **56a**, the title compound **56c** was obtained as a colorless oil in a reaction with a 65% yield using **23c** instead of **23a**.

¹H NMR (400 MHz, CDCl₃) δ ppm 1.35–1.65 (m, 13H), 1.76–1.89 (m, 1H), 2.22–2.35 (m, 5H), 2.39–2.50 (m, 1H), 2.56–2.73 (m, 2H), 2.78–2.91 (m, 1H), 2.93–3.05 (m, 1H), 3.20 (s, 3H), 3.73–3.82 (m, 5H), 3.94–4.10 (m, 2H), 4.11–4.19 (m, 2H), 4.43–4.51 (m, 4H), 5.53 (brs, 1H), 5.77–5.85 (m, 1H), 6.16–6.20 (m, 1H), 6.77 (d, *J* = 8.44 Hz, 1H), 7.27–7.39 (m, 6H), 7.66 (s, 1H), 8.33–8.45 (m, 1H), MS (ESI/APCI dual) *m/z*: 741 [M + H]⁺

5.2.10. (18*aS*)-13-[(1*S*,3*R*)-3-(benzyloxy)cyclobutyl]-2-fluoro-11-methyl-8,9,10,11,19,20,21,22-octahydro-18*aH*,24*H*-18,15-(metheno)pyrido[2,1-*l*]pyrimido[6,1-*h*][1,4,7,9,10,13]benzoxapentaazacyclohexadecine-7,24(6*H*)-dione (**58a**)

To a solution of **56a** (0.11 g, 0.145 mmol) in methanol (0.5 mL) and THF (0.5 mL) was added 1 M aqueous sodium hydroxide (1.0 mL), and the mixture was stirred at room temperature for 0.5 h. The reaction mixture was acidified using 1 M aqueous hydrochloric acid and extracted with chloroform. The organic layer was washed with brine, dried over magnesium sulfate, filtered, and concentrated under reduced pressure to obtain 2-[2-[2-[[5-(3-benzyloxycyclobutyl)-2-[(2*S*)-1-*tert*-butoxycarbonyl-2-piperidyl]pyrazolo[1,5-*a*]pyrimidin-7-yl]methylamino]ethylamino]-2-oxoethoxy]-5-fluorobenzoic acid (0.10 g, 0.141 mmol, 97%) as a colorless oil. This compound was used in the next reaction without further purification.

To a solution of 2-[2-[2-[[5-(3-benzyloxycyclobutyl)-2-[(2*S*)-1-*tert*-butoxycarbonyl-2-piperidyl]pyrazolo[1,5-*a*]pyrimidin-7-yl]methylamino]ethylamino]-2-oxoethoxy]-5-fluorobenzoic acid (0.10 g, 0.141 mmol) in 1,4-dioxane (0.24 mL) was added 4 M hydrogen chloride in 1,4-dioxane (0.47 mL). After stirring for 1 h at room temperature, the reaction mixture was concentrated under reduced pressure to obtain **57a** (96 mg, 0.144 mmol, quant.) as a colorless powder. This compound was used in the next reaction without further purification.

To a solution of **57a** (96 mg, 0.141 mmol) in *N,N*-dimethylformamide (7.2 mL, 0.02 M) was added triethylamine (0.16 mL, 1.15 mmol, 8.0 eq) and 1-[bis(dimethylamino)methylene]-1*H*-1,2,3-triazolo[4,5-*b*]pyridinium 3-oxide hexafluorophosphate (0.11 g, 0.288 mmol, 2.0 eq). After stirring at room temperature for 2 h, the reaction mixture was poured into saturated aqueous sodium bicarbonate and extracted with ethyl acetate. The organic layer was washed with brine, dried over magnesium sulfate, filtered, and concentrated under reduced pressure. The residue was purified using silica gel column chromatography (NH 50%–90% ethyl acetate in hexane) to obtain **58a** (72 mg, 0.118 mmol, 82%) as colorless amorphous substance.

¹H NMR (400 MHz, CDCl₃) δ ppm 1.63–1.92 (m, 3H), 1.96–2.44 (m, 4H), 2.63–2.75 (m, 2H), 2.86–3.32 (m, 8H), 4.02–4.32 (m, 2H), 4.33–4.60 (m, 4H), 4.71–4.81 (m, 0.6H), 4.87–5.10 (m, 2H), 5.99 (s, 0.6H), 6.04 (s, 0.4H), 6.25 (s, 0.6H), 6.31–6.38 (m, 0.4H), 6.58 (s, 0.4H), 6.80–6.89 (m, 1H), 6.97–7.09 (m, 2H), 7.29–7.40 (m, 5H), 7.75–7.82 (m, 0.4H), 8.95–9.02 (m, 0.6H), MS (ESI/APCI dual) *m/z*: 613 [M + H]⁺

5.2.11. (18*aS*)-13-[(1*S*,3*R*)-3-(benzyloxy)cyclobutyl]-2-chloro-11-methyl-8,9,10,11,19,20,21,22-octahydro-18*aH*,24*H*-18,15-(metheno)pyrido[2,1-*l*]pyrimido[6,1-*h*][1,4,7,9,10,13]benzoxapentaazacyclohexadecine-7,24(6*H*)-dione (**58b**)

According to the procedure described for **58a**, the title compound **58b** was obtained from **56b** as a colorless amorphous substance in a reaction with an 89% yield.

¹H NMR (400 MHz, CDCl₃) δ ppm 1.63–1.93 (m, 3H), 1.95–2.43 (m,

4H), 2.61–2.77 (m, 2H), 2.84–3.32 (m, 8H), 4.02–4.31 (m, 2H), 4.33–4.59 (m, 4H), 4.70–4.80 (m, 0.6H), 4.84–5.06 (m, 2H), 5.98 (s, 0.6H), 6.04 (s, 0.4H), 6.26 (s, 0.6H), 6.31–6.37 (m, 0.4H), 6.57 (s, 0.4H), 6.77–6.86 (m, 1H), 7.28–7.39 (m, 7H), 7.72–7.80 (m, 0.4H), 8.80–8.91 (m, 0.6H), MS (ESI/APCI dual) m/z : 629 [M + H]⁺

5.2.12. (18aS)-13-[(1*s*,3*R*)-3-(Benzyloxy)cyclobutyl]-2,11-dimethyl-8,9,10,11,19,20,21,22-octahydro-18aH,24H-18,15-(metheno)pyrido[2,1-*l*]pyrimido[6,1-*h*][1,4,7,9,10,13]benzoxapentaazacyclohexadecine-7,24(6H)-dione (58c)

According to the procedure described for **58a**, the title compound **58c** was obtained from **56c** as a colorless amorphous substance in a reaction with an 89% yield.

MS (ESI/APCI dual) m/z : 609 [M + H]⁺

5.2.13. (18aS)-2-Fluoro-13-[(1*s*,3*R*)-3-hydroxycyclobutyl]-11-methyl-8,9,10,11,19,20,21,22-octahydro-18aH,24H-18,15-(metheno)pyrido[2,1-*l*]pyrimido[6,1-*h*][1,4,7,9,10,13]benzoxapentaazacyclohexadecine-7,24(6H)-dione (59a)

To a solution of **58a** (72 mg, 0.118 mmol) in methanol (1.2 mL) was added palladium hydroxide on carbon (36 mg). The reaction was flushed with hydrogen and stirred under a hydrogen atmosphere at 60 °C for 3 h. The reaction mixture was cooled to room temperature and filtered through a pad of Celite®, then concentrated under reduced pressure. The residue was purified using silica gel column chromatography (NH chloroform) to obtain **59a** (56 mg, 0.11 mmol, 91%) as a colorless amorphous substance.

¹H NMR (600 MHz, DMSO-*d*₆) δ ppm 1.40–1.85 (m, 4H), 1.86–2.05 (m, 1H), 2.07–2.30 (m, 3H), 2.44–2.55 (m, 1H), 2.89–3.23 (m, 6H), 3.34–3.53 (m, 1H), 3.88–3.97 (m, 0.3H), 3.98–4.09 (m, 2.4H), 4.20–4.27 (m, 0.3H), 4.47–4.57 (m, 1.7H), 4.60–4.66 (m, 0.3H), 4.82–4.94 (m, 1.4H), 5.09–5.14 (m, 1H), 6.07–6.10 (m, 0.3H), 6.15–6.19 (m, 0.7H), 6.21–6.24 (m, 0.3H), 6.32–6.36 (m, 0.7H), 6.56–6.59 (m, 0.3H), 7.08–7.12 (m, 0.7H), 7.15–7.28 (m, 1.6H), 7.34–7.38 (m, 0.7H), 7.52–7.56 (m, 0.3H), 8.85–8.90 (m, 0.7H), ¹³C NMR (151 MHz, DMSO-*d*₆) δ ppm 19.8, 24.7, 29.7, 31.9, 36.4, 36.6, 38.0, 40.0, 43.6, 48.1, 54.0, 61.5, 71.0, 91.0, 92.4, 113.7, 116.5, 119.8, 130.6, 149.3, 149.6, 151.6, 154.2, 156.9, 164.3, 165.5, 167.5, HRMS ESI/APCI dual m/z calcd for C₂₇H₃₁FN₆O₄ [M + H]⁺ 523.2464, found: 523.2454

5.2.14. (18aS)-2-Chloro-13-[(1*s*,3*R*)-3-hydroxycyclobutyl]-11-methyl-8,9,10,11,19,20,21,22-octahydro-18aH,24H-18,15-(metheno)pyrido[2,1-*l*]pyrimido[6,1-*h*][1,4,7,9,10,13]benzoxapentaazacyclohexadecine-7,24(6H)-dione (59b)

To a solution of **58b** (4.5 g, 7.20 mmol) in acetonitrile (72 mL) was added chlorotrimethylsilane (4.6 mL, 36.0 mmol, 5.0 eq) and sodium iodide (5.4 g, 36.0 mmol, 5.0 eq). After stirring at 65 °C for 1 h, the reaction mixture was poured into saturated aqueous sodium thiosulfate/saturated aqueous sodium bicarbonate (1/1) and extracted with ethyl acetate. The organic layer was washed with brine, dried over magnesium sulfate, filtered, and concentrated under reduced pressure. The residue was purified using silica gel column chromatography (OH 0%–20% methanol in chloroform) and silica gel column chromatography (NH 0%–12% methanol in chloroform) to obtain **59b** (3.6 g, 6.75 mmol, 94%) as colorless amorphous substance.

¹H NMR (400 MHz, CDCl₃) δ ppm 1.42–2.29 (m, 6.6H), 2.34–2.43 (m, 0.4H), 2.72–2.85 (m, 2H), 2.86–3.32 (m, 8H), 4.17–4.59 (m, 4.4H), 4.70–4.80 (m, 0.6H), 4.88–5.10 (m, 1.6H), 5.95 (s, 0.6H), 6.01 (s, 0.4H), 6.25 (s, 0.6H), 6.30–6.37 (m, 0.4H), 6.57 (s, 0.4H), 6.77–6.86 (m, 1H), 7.27–7.34 (m, 2H), 7.76 (d, *J* = 7.82 Hz, 0.4H), 8.84 (d, *J* = 7.58 Hz, 0.6H), MS (ESI/APCI dual) m/z : 539 [M + H]⁺

5.2.15. (18aS)-13-[(1*s*,3*R*)-3-Hydroxycyclobutyl]-2,11-dimethyl-8,9,10,11,19,20,21,22-octahydro-18aH,24H-18,15-(metheno)pyrido[2,1-*l*]pyrimido[6,1-*h*][1,4,7,9,10,13]benzoxapentaazacyclohexadecine-7,24(6H)-dione (59c)

According to the procedure described for **59a**, the title compound **59c** was obtained from **58c** as a colorless amorphous substance in a reaction with an 87% yield.

¹H NMR (400 MHz, CDCl₃) δ ppm 1.60–2.43 (m, 7H), 2.73–3.36 (m, 10H), 4.17–4.58 (m, 4.4H), 4.73–4.83 (m, 0.6H), 4.90–5.14 (m, 1.6H), 5.92–5.96 (m, 0.6H), 5.97–6.01 (m, 0.4H), 6.24 (s, 0.6H), 6.34–6.41 (m, 0.4H), 6.57 (s, 0.4H), 6.77 (d, *J* = 8.07 Hz, 1H), 7.07–7.17 (m, 2H), 7.77–7.86 (m, 0.4H), 8.91–9.03 (m, 0.6H), MS (ESI/APCI dual) m/z : 519 [M + H]⁺

5.2.16. (18aS)-2-Fluoro-13-[(1*r*,3*S*)-3-hydroxycyclobutyl]-11-methyl-8,9,10,11,19,20,21,22-octahydro-18aH,24H-18,15-(metheno)pyrido[2,1-*l*]pyrimido[6,1-*h*][1,4,7,9,10,13]benzoxapentaazacyclohexadecine-7,24(6H)-dione (60a)

To a solution of **59a** (55 mg, 0.11 mmol) in THF (1.1 mL) was added 4-nitrobenzoic acid (26 mg, 0.158 mmol, 1.5 eq), 2.2 M diethyl azodicarboxylate in toluene (0.29 mL, 0.632 mmol, 6.0 eq) and triphenylphosphine (0.17 g, 0.632 mmol, 6.0 eq). After stirring at 65 °C for 30 min, the reaction mixture was cooled to room temperature and concentrated under reduced pressure. The residue was purified using silica gel column chromatography (NH 50%–100% ethyl acetate in hexane) to obtain (1*S*,3*r*)-3-[(18a*S*)-2-fluoro-11-methyl-7,24-dioxo-6,7,8,9,10,11,19,20,21,22-decahydro-18aH,24H-18,15-(metheno)pyrido[2,1-*l*]pyrimido[6,1-*h*][1,4,7,9,10,13]benzoxapentaazacyclohexadecine-13-yl]cyclobutyl 4-nitrobenzoate (74 mg, 0.11 mmol, quant.) as colorless amorphous substance.

MS (ESI/APCI dual) m/z : 672 [M + H]⁺

To a solution of (1*S*,3*r*)-3-[(18a*S*)-2-fluoro-11-methyl-7,24-dioxo-6,7,8,9,10,11,19,20,21,22-decahydro-18aH,24H-18,15-(metheno)pyrido[2,1-*l*]pyrimido[6,1-*h*][1,4,7,9,10,13]benzoxapentaazacyclohexadecine-13-yl]cyclobutyl 4-nitrobenzoate (73 mg, 0.11 mmol) in THF (1.1 mL) was added 1 M aqueous sodium hydroxide (1.1 mL), and the mixture was stirred at room temperature for 1.5 h. The reaction mixture was neutralized by 1 M aqueous hydrochloric acid and extracted with chloroform. The organic layer was dried over magnesium sulfate, filtered, and concentrated under reduced pressure. The residue was purified using silica gel column chromatography (OH 0%–5% methanol in chloroform) to obtain **60a** (41 mg, 0.078 mmol, 72%) as a colorless amorphous substance.

¹H NMR (600 MHz, DMSO-*d*₆) δ ppm 1.41–1.86 (m, 4H), 1.86–2.06 (m, 1H), 2.14–2.30 (m, 3H), 2.44–2.55 (m, 1H), 2.93 (s, 0.9H), 2.98 (s, 2.1H), 3.01–3.22 (m, 3H), 3.34–3.53 (m, 1.6H), 3.87–3.97 (m, 0.3H), 3.98–4.10 (m, 1.4H), 4.20–4.29 (m, 0.3H), 4.33–4.43 (m, 1H), 4.48–4.58 (m, 1.4H), 4.60–4.65 (m, 0.3H), 4.82–4.95 (m, 1.4H), 5.03–5.09 (m, 1H), 6.06–6.10 (m, 0.3H), 6.16 (s, 0.7H), 6.22 (s, 0.3H), 6.35 (s, 0.7H), 6.58 (s, 0.3H), 7.09–7.13 (m, 0.7H), 7.16–7.29 (m, 1.6H), 7.35–7.38 (m, 0.7H), 7.53–7.56 (m, 0.3H), 8.88 (d, *J* = 7.02 Hz, 0.7H), ¹³C NMR (151 MHz, DMSO-*d*₆) δ ppm 19.8, 24.7, 29.7, 33.9, 36.6, 37.7, 38.0, 40.0, 43.6, 48.1, 54.0, 63.9, 71.0, 91.3, 92.5, 113.7, 116.5, 119.8, 130.5, 149.6, 150.4, 151.6, 154.2, 156.9, 165.5, 165.7, 167.5, HRMS ESI/APCI dual m/z calcd for C₂₇H₃₁FN₆O₄ [M + H]⁺ 523.2464, found: 523.2450

5.2.17. (18aS)-2-Chloro-13-[(1*r*,3*S*)-3-hydroxycyclobutyl]-11-methyl-8,9,10,11,19,20,21,22-octahydro-18aH,24H-18,15-(metheno)pyrido[2,1-*l*]pyrimido[6,1-*h*][1,4,7,9,10,13]benzoxapentaazacyclohexadecine-7,24(6H)-dione (60b)

According to the procedure described for **60a**, the title compound **60b** was obtained from **59b** as a colorless amorphous substance in a reaction with a 54% yield.

¹H NMR (600 MHz, DMSO-*d*₆) δ ppm 1.43–1.85 (m, 4H), 1.87–1.96 (m, 0.7H), 1.97–2.05 (m, 0.3H), 2.14–2.29 (m, 3H), 2.44–2.55 (m, 1H),

2.93 (s, 0.9H), 2.98 (s, 2.1H), 3.03–3.23 (m, 2.7H), 3.37–3.57 (m, 1.6H), 3.86–3.94 (m, 0.3H), 4.01–4.08 (m, 0.7H), 4.11 (d, $J = 14.04$ Hz, 0.7H), 4.16–4.22 (m, 0.3H), 4.34–4.44 (m, 1H), 4.50–4.56 (m, 1.7H), 4.65 (d, $J = 14.86$ Hz, 0.3H), 4.83–4.91 (m, 1.4H), 5.04–5.08 (m, 1H), 6.05–6.09 (m, 0.3H), 6.16 (s, 0.7H), 6.22 (s, 0.3H), 6.36 (s, 0.7H), 6.58 (s, 0.3H), 7.08 (d, $J = 8.67$ Hz, 0.7H), 7.19 (d, $J = 8.67$ Hz, 0.3H), 7.39–7.46 (m, 1.3H), 7.51–7.55 (m, 1H), 8.73 (d, $J = 7.43$ Hz, 0.7H), ^{13}C NMR (151 MHz, DMSO- d_6) δ ppm 19.8, 24.7, 29.7, 33.9, 36.7, 37.7, 38.1, 43.6, 48.2, 54.1, 63.9, 70.0, 79.1, 91.3, 92.6, 118.8, 126.4, 129.8, 130.4, 149.5, 151.6, 151.9, 154.1, 155.5, 165.4, 165.6, 167.3, HRMS ESI/APCI dual m/z calcd for $\text{C}_{27}\text{H}_{31}\text{ClN}_6\text{O}_4$ [$\text{M} + \text{H}$] $^+$ 539.2168, found: 539.2152

5.2.18. (18a*S*)-13-[(1*r*,3*S*)-3-Hydroxycyclobutyl]-2,11-dimethyl-8,9,10,11,19,20,21,22-octahydro-18a*H*,24*H*-18,15-(metheno)pyrido[2,1-*l*]pyrimido[6,1-*h*][1,4,7,9,10,13]benzoxapentaazacyclohexadecine-7,24(6*H*)-dione (60*c*)

According to the procedure described for 60*a*, the title compound 60*c* was obtained from 59*c* as a colorless amorphous substance in a reaction with a 96% yield.

^1H NMR (600 MHz, DMSO- d_6) δ ppm 1.37–1.88 (m, 4.7H), 1.92–2.02 (m, 0.3H), 2.07–2.26 (m, 3H), 2.28 (s, 0.9H), 2.30 (s, 2.1H), 2.45–2.55 (m, 1H), 2.90–3.01 (m, 3H), 3.02–3.17 (m, 2.6H), 3.20–3.26 (m, 0.3H), 3.36–3.58 (m, 1.4H), 3.84–3.92 (m, 0.3H), 3.97–4.08 (m, 1.7H), 4.16–4.24 (m, 0.3H), 4.33–4.43 (m, 0.7H), 4.44–4.49 (m, 1H), 4.53–4.62 (m, 1H), 4.83–4.92 (m, 1.4H), 5.03–5.15 (m, 1H), 6.07–6.11 (m, 0.3H), 6.14–6.18 (m, 0.7H), 6.20–6.23 (m, 0.3H), 6.33–6.38 (m, 0.7H), 6.54–6.58 (m, 0.3H), 6.92–6.95 (m, 0.7H), 7.01–7.04 (m, 0.3H), 7.10–7.20 (m, 2H), 7.54–7.60 (m, 0.3H), 8.86–8.92 (m, 0.7H), ^{13}C NMR (151 MHz, DMSO- d_6) δ ppm 19.8, 20.1, 24.9, 29.8, 33.9, 36.6, 37.7, 40.0, 43.5, 48.1, 54.0, 63.9, 70.7, 79.1, 91.2, 92.5, 117.6, 126.9, 128.8, 130.4, 132.7, 149.5, 151.1, 151.6, 154.3, 165.7, 167.1, 167.7, HRMS ESI/APCI dual m/z calcd for $\text{C}_{28}\text{H}_{34}\text{N}_6\text{O}_4$ [$\text{M} + \text{H}$] $^+$ 519.2714, found: 519.2706

5.3. NMR analysis

For the EXSY (EXchange Spectroscopy) analysis,^{47,48} each compound was dissolved in DMSO- d_6 at 10 mg/mL. Spectra were recorded using a JNM-ECA500 spectrometer (JEOL) with a mixing time of 0.5 s and relaxation delay of 10 s. Compounds 42*c* and 60*b* produced clear exchange signals sufficient for analysis at room temperature. Furthermore, the exchange rates for 42*a*, which showed no exchange signals at room temperature, were predicted by extrapolating an Arrhenius plot from 60 °C to 90 °C. The detailed calculation method of rotational half-lives of the compounds (42*a*, 42*c*, 60*b*) and their EXSY spectra are described in [Supporting Information](#).

6. Biological assay protocols

6.1. Cells and viruses

HEp-2 cells were purchased from DS Pharma Biomedical Co., Ltd. (Osaka, Japan) and cultured in minimum essential medium (MEM) supplemented with 10% fetal bovine serum (FBS), 50 $\mu\text{g}/\text{mL}$ gentamicin, and 600 $\mu\text{g}/\text{mL}$ L-glutamine. RSV A2 (ATCC VR-1540) was purchased from the American Type Culture Collection (Manassas, VA, USA). RSV A2 with the D486N mutation in F protein was selected by serial passage in the presence of a pyrazolo[1,5-*a*]pyrimidine derivative 9*c* (*N*-[(1*S*)-1-{5-[(3*S*)-3-aminopyrrolidin-1-yl]-6-methylpyrazolo[1,5-*a*]pyrimidin-2-yl}propyl]-5-chloro-2-[(methanesulfonyl)amino]-*N*-methylbenzamide), as described in our previous report.⁴⁵ The mutant was confirmed to have no other mutations in the F gene by a genotypic analysis.

6.2. Antiviral assay

HEp-2 cells were cultured in 96-well plates overnight, and the test compounds were added after dilution with MEM supplemented with 2% FBS, 100 units/mL penicillin, 100 $\mu\text{g}/\text{mL}$ streptomycin and 300 $\mu\text{g}/\text{mL}$ L-glutamine. The cells were then infected with RSV A2 or D486N. After incubation at 37 °C, 5% CO_2 for 4 d, the RSV-induced CPE was determined by adding XTT reagent. The concentration of the test compound required to inhibit the CPE by 50% (EC_{50}) was calculated using the least squares method.

6.3. Molecular docking and molecular dynamics simulation

A molecular docking simulation of compound 60*b* with RSV A2 was performed using the CDOCKER algorithm in Discovery Studio 2017 R2. The input coordinates of RSV A2 were obtained from the X-ray coordinates of RSV A2 complexed with its inhibitor JNJ-2408068 (PDB entry 5EA3). The “Input Site Sphere” parameter for CDOCKER was defined using the position of JNJ-2408068. Hydrogen atoms were added, and the ionization states were assigned using the Protonate-3D function of the Molecular Operating Environment program (MOE);⁴⁹ the positions of the hydrogen atoms were then optimized using the Amber10 forcefield implemented in MOE.

The molecular dynamics (MD) simulation was performed using the Standard Dynamics Cascade algorithm in Discovery Studio 2017 R2.⁵⁰ The input coordinates were obtained from the result of the molecular docking simulation of RSV A2 and compound 60*b*. A CHARMM forcefield and GBSW model were applied to the compounds and solvent, respectively. A production MD of 1.0 ns was performed using the well-equilibrated system at a temperature of 300 K.

6.4. Parallel artificial membrane permeability assay (PAMPA)

Membrane permeability was evaluated using the PAMPA Evolution instrument (pION Inc., Billerica, MA, USA). The permeation of a test compound across an artificial membrane was quantified using a UV plate reader after 4 h of incubation at room temperature. The apparent permeability at pH6.2 was calculated using PAMPA Evolution software (pION Inc.).

6.5. Metabolism-dependent inhibition (MDI)

A test compound was pre-incubated for 0 or 30 min with 10 \times HLMs (0.5 mg protein/mL) at 37 °C in sodium-potassium phosphate buffer (pH7.4) containing a β -nicotinamide-adenine dinucleotide phosphate (NADPH)-regenerating system. At the end of the pre-incubation period, an aliquot of the reaction mixture was diluted (10-fold) into a secondary incubation buffer containing a probe substrate for CYP3A (testosterone, 250 μM) and a β -NADPH-regenerating system. Secondary incubation was performed for 10 min, and the reaction was terminated by the addition of acetonitrile containing an internal standard. The precipitated protein was removed by centrifugation, and the supernatant was subjected to liquid chromatography/tandem mass spectrometry. The percent inhibition of probe metabolism with 0-min or 30-min of pre-incubation was calculated, and the metabolic-dependent inhibition was calculated as the percent inhibition difference between 0-min and 30-min of pre-incubation.

6.6. Plasma protein binding

The protein binding of the test compounds in human and mouse plasma was evaluated using the equilibrium dialysis method. Equilibrium dialysis was conducted on a 96-well Equilibrium Dialysis Device (HTDialysis, LLC, Gales Ferry, CT, USA) with a 12 to 14-kDa cutoff dialysis membrane. A test compound was dissolved in DMSO and spiked into the blank plasma at a final concentration of 1 $\mu\text{g}/\text{mL}$. The plasma

sample was equilibrated with phosphate buffer (pH7.4) at 37 °C in 5% CO₂ for 4 h. After dialysis, the concentrations of the test compound in plasma and phosphate buffer were determined using a liquid chromatography-tandem mass spectrometry method. The protein binding (%) was calculated based on the instruction manual for the 96-well plate.

Declaration of Competing Interest

The authors declare that they have no known competing financial interests or personal relationships that could have appeared to influence the work reported in this paper.

Acknowledgments

The authors thank Dr. Taiji Asami for carefully reading the manuscript and making useful suggestions to improve it, Dr. Takashi Yoshizumi and Mr. Susumu Yamanobe for their helpful discussions, and Mr. Akira Higuchi for his assistance with the analytical and spectrum studies.

Appendix A. Supplementary material

Supplementary data to this article can be found online at <https://doi.org/10.1016/j.bmc.2020.115818>.

References

- Blount REJ, Morris JA, Savage RE. Recovery of cytopathogenic agent from chimpanzees with coryza. *Proc. Soc. Exp. Biol. Med.* 1956;92:544–549. <https://doi.org/10.3181/00379727-92-22538>.
- Sigurs N, Bjarnason R, Sigurbjörgsson F, Kjellman B. Respiratory syncytial virus bronchiolitis in infancy is an important risk factor for asthma and allergy at age 7. *Am. J. Respir. Crit. Care Med.* 2000;161:1501–1507. <https://doi.org/10.1164/ajrccm.161.5.9906076>.
- Sigurs N, Aljassim F, Kjellman B, et al. Asthma and allergy patterns over 18 years after severe RSV bronchiolitis in the first year of life. *Thorax.* 2010;65:1045–1052. <https://doi.org/10.1136/thx.2009.121582>.
- Sigurs N, Gustafsson PM, Bjarnason R, et al. Severe respiratory syncytial virus bronchiolitis in infancy and asthma and allergy at age 13. *Am. J. Respir. Crit. Care Med.* 2005;171:137–141. <https://doi.org/10.1164/rccm.200406-7300C>.
- Stein RT, Sherrill D, Morgan WJ, et al. Respiratory syncytial virus in early life and risk of wheeze and allergy by age 13 years. *Lancet.* 1999;354:541–545. [https://doi.org/10.1016/S0140-6736\(98\)10321-5](https://doi.org/10.1016/S0140-6736(98)10321-5).
- Bont L, Steijn M, van Aalderen WM, Kimpen JL. Impact of wheezing after respiratory syncytial virus infection on health-related quality of life. *Pediatr. Infect. Dis. J.* 2004; 23:414–417. <https://doi.org/10.1097/01.inf.0000122604.32137.29>.
- Henderson J, Hilliard TN, Sherriff A, Stalker D, Al Shammari N, Thomas HM. Hospitalization for RSV bronchiolitis before 12 months of age and subsequent asthma, atopy and wheeze: a longitudinal birth cohort study. *Pediatr. Allergy Immunol.* 2005;16:386–392. <https://doi.org/10.1542/peds.2006.0900J>.
- Nair H, Nokes DJ, Gessner BD, et al. Global burden of acute lower respiratory infections due to respiratory syncytial virus in young children: a systematic review and meta-analysis. *Lancet.* 2010;375:1545–1555. [https://doi.org/10.1016/S0140-6736\(10\)6206-1](https://doi.org/10.1016/S0140-6736(10)6206-1).
- Lozano R, Naghavi M, Foreman K, et al. Global and regional mortality from 235 causes of death for 20 age groups in 1990 and 2010: a systematic analysis for the Global Burden of Disease Study 2010. *Lancet.* 2012;380:2095–2128. [https://doi.org/10.1016/S0140-6736\(12\)61728-0](https://doi.org/10.1016/S0140-6736(12)61728-0).
- Resch B, Manzoni P, Lanari M. Severe respiratory syncytial virus (RSV) infection in infants with neuromuscular diseases and immune deficiency syndromes. *Paediatr. Respir. Rev.* 2009;10:148–153. <https://doi.org/10.1016/j.prrv.2009.06.003>.
- Hall CB, Powell KR, MacDonald NE, et al. Respiratory syncytial viral infection in children with compromised immune function. *N. Engl. J. Med.* 1986;315:77–81. <https://doi.org/10.1056/NEJM198607103150201>.
- Shi T, McAllister DA, O'Brien KL, et al. RSV Global Epidemiology Network, Global, regional, and national disease burden estimates of acute lower respiratory infections due to respiratory syncytial virus in young children in 2015: a systematic review and modelling study. *Lancet.* 2017;390:946–958. [https://doi.org/10.1016/S0140-6736\(17\)30938-8](https://doi.org/10.1016/S0140-6736(17)30938-8).
- Weiss RA, McMichael AJ. Social and environmental risk factors in the emergence of infectious diseases. *Nat. Med.* 2004;10:S70–76. <https://doi.org/10.1038/nm1150>.
- Smith DK, Seales S, Budzik C. Respiratory syncytial virus bronchiolitis in children. *Am. Fam. Physician.* 2017;95:94–99.
- Kou M, Hwang V, Ramkellawan N. Bronchiolitis: from practice guideline to clinical practice. *Emerg. Med. Clin. North. Am.* 2018;36:275–286. <https://doi.org/10.1016/j.emc.2017.12.006>.
- Offer I, Ashkenazi S, Livni G, Shalit I. The diagnostic and therapeutic approach to acute bronchiolitis in hospitalized children in Israel: a nationwide survey. *Isr. Med. Assoc. J.* 2000;2:108–110.
- Livni G, Rachmel A, Marom D, Yaari A, Tirosh N, Ashkenazi S. A randomized, double-blind study examining the comparative efficacies and safety of inhaled epinephrine and nasal decongestant in hospitalized infants with acute bronchiolitis. *Pediatr. Infect. Dis. J.* 2010;29:71–73. <https://doi.org/10.1097/INF.0b013e3181b0602e>.
- Meissner HC. Viral bronchiolitis in children. *N. Engl. J. Med.* 2016;374:62–72. <https://doi.org/10.1056/NEJMra1413456>.
- Palivizumab, a humanized respiratory syncytial virus monoclonal antibody, reduces hospitalization from respiratory syncytial virus infection in high-risk infants. The impact-RSV study group. *Pediatrics.* 1998, 102, 531–537.
- Wu P, Escobar GJ, Gebretsadik T, et al. Effectiveness of respiratory syncytial virus immunoprophylaxis on bronchiolitis hospitalizations among high-risk infants. *Am. J. Epidemiol.* 2018;187:1490–1500. <https://dx.doi.org/10.1093%2Faje%2Fkwy008>.
- Obando-Pacheco P, Justicia-Grande AJ, Rivero-Calle I, et al. Respiratory syncytial virus seasonality: A global overview. *J. Infect. Dis.* 2018;217:1356–1364. <https://doi.org/10.1093/infdis/jiy056>.
- Revankar GR, Robins RK. Synthesis and biological activity of some nucleosides resembling guanosine: imidazo(1,2- α)pyrimidine nucleosides. *Ann. NY Acad. Sci.* 1975;255:166–176. <https://doi.org/10.1111/j.1749-6632.1975.tb29221.x>.
- Sidwell RW, Huffman JH, Khare GP, Allen LB, Witkowski JT, Robins RK. Broad-spectrum antiviral activity of virazole: 1- β -D-ribofuranosyl-1,2,4-triazole-3-carboxamide. *Science.* 1972;177:705–706. <https://doi.org/10.1126/science.177.4050.705>.
- Hall CB, Walsh EE, Hruska JF, Betts RF, Hall WJ. Ribavirin treatment of experimental respiratory syncytial viral infection. A controlled double-blind study in young adults. *JAMA.* 1983;249:2666–2670.
- Streeter DG, Witkowski JT, Khare GP, et al. Mechanism of action of 1- β -D-ribofuranosyl-1,2,4-triazole-3-carboxamide (Virazole), a new broad-spectrum antiviral agent. *Proc. Natl. Acad. Sci. U S A.* 1973;70:1174–1178. <https://doi.org/10.1073/pnas.70.4.1174>.
- Ohmit SE, Moler FW, Monto AS, Khan AS. Ribavirin utilization and clinical effectiveness in children hospitalized with respiratory syncytial virus infection. *J. Clin. Epidemiol.* 1996;49:963–967. [https://doi.org/10.1016/0895-4356\(96\)00137-0](https://doi.org/10.1016/0895-4356(96)00137-0).
- Graci JD, Cameron CE. Mechanisms of action of ribavirin against distinct viruses. *Rev. Med. Virol.* 2006;16:37–48. <https://doi.org/10.1002/rmv.483>.
- Hultgren C, Milich DR, Weiland O, Sällberg M. The antiviral compound ribavirin modulates the T helper (Th) 1/Th2 subset balance in hepatitis B and C virus-specific immune responses. *J. Gen. Virol.* 1998;79:2381–2391. <https://doi.org/10.1099/0022-1317-79-10-2381>.
- Mackman RL, Sangi M, Sperandio D, et al. Discovery of an oral respiratory syncytial virus (RSV) fusion inhibitor (GS-5806) and clinical proof of concept in a human RSV challenge study. *J. Med. Chem.* 2015;58:1630–1643. <https://doi.org/10.1021/jm5017768>.
- Babaoglu K, Eisenberg EJ, Mackman RL, Sangi M, Siegel D, Yang H. Pyrazolo[1,5-a]pyrimidines as antiviral agents. World Intellectual Property Organization, WO/2011/163518, 2011.
- Tahri A, Vendeville SMH, Jonckers THM, Raboisson PJM, Demin SD, Hu L, Coymans LP. Piperidine Substituted Pyrazolo[1,5-a]pyrimidine Derivatives with Inhibitory Activity on the Replication of the Respiratory Syncytial Virus (RSV). World Intellectual Property Organization, WO/2016/091774, 2016.
- Tahri A, Vendeville SMH, Jonckers THM, Raboisson PJM, Demin SD, Hu L. Piperidine Substituted Tricyclic Pyrazolo[1,5-a]pyrimidine Derivatives with Inhibitory Activity on the Replication of the Respiratory Syncytial Virus (RSV). World Intellectual Property Organization, WO/2016/091791, 2016.
- Shi W, Jiang Z, He H, et al. Discovery of 3,3'-spiro[azetidine]-2-oxindoline derivatives as fusion inhibitors for treatment of RSV infection. *ACS Med. Chem. Lett.* 2018;9:94–97. <https://doi.org/10.1021/acsmchemlett.7b00418>.
- Feng S, Hong D, Wang B, et al. Discovery of imidazopyridine derivatives as highly potent respiratory syncytial virus fusion inhibitors. *ACS Med. Chem. Lett.* 2015;6: 359–362. <https://doi.org/10.1021/acsmchemlett.5b00008>.
- Feng S, Li C, Chen D, et al. Discovery of methylsulfonyl indazoles as potent and orally active respiratory syncytial virus (RSV) fusion inhibitors. *Eur. J. Med. Chem.* 2017; 138:1147–1157. <https://doi.org/10.1016/j.ejmech.2017.07.032>.
- Zheng X, Wang L, Wang B, et al. Discovery of piperazinylquinoline derivatives as novel respiratory syncytial virus fusion inhibitors. *ACS Med. Chem. Lett.* 2016;7: 558–562. <https://doi.org/10.1021/acsmchemlett.5b00234>.
- Stray K, Perron M, Porter DP, et al. Drug resistance assessment following administration of RSV fusion inhibitor presatovir to participants experimentally infected with respiratory syncytial virus. *J. Infect. Dis.* 2020;jiaa028. <https://doi.org/10.1093/infdis/jiaa028>.
- Porter DP, Guo Y, Perry J, et al. Assessment of drug resistance during phase 2b clinical trials of presatovir in adults naturally infected with respiratory syncytial virus. *Antimicrob Agents Chemother.* 2020;02312–02319.
- Perron M, Stray K, Kinkade A, et al. GS-5806 inhibits a broad range of respiratory syncytial virus clinical isolates by blocking the virus-cell fusion process. *Antimicrob Agents Chemother.* 2015;60:1264–1273. <https://doi.org/10.1128/AAC.01497-15>.
- Roymans D, De Bondt HL, Arnoult E, et al. Binding of a potent small-molecule inhibitor of six-helix bundle formation requires interactions with both heptad-repeats of the RSV fusion protein. *Proc. Natl. Acad. Sci. U S A.* 2010;107:308–313. <https://doi.org/10.1073/pnas.0910108106>.

- 41 Yamaguchi ST, Tokura S, Ogata Y, et al. Discovery of a Potent Dual Inhibitor of Wild-Type and Mutant Respiratory Syncytial Virus Fusion Proteins. *ACS Med. Chem. Lett.* 2020;11:1145–1151. <https://doi.org/10.1021/acsmchemlett.0c00008>.
- 42 Laplante SR, Fader LD, Fandrick KR, et al. Assessing Atropisomer Axial Chirality in Drug Discovery and Development. *J. Med. Chem.* 2011;54:7005–7022. <https://doi.org/10.1021/jm200584g>.
- 43 LaPlante SR, Edwards PJ, Fader LD, Jakalian A, Hucke O. Revealing atropisomer axial chirality in drug discovery. *ChemMedChem.* 2011;6:505–513. <https://doi.org/10.1002/cmdc.201000485>.
- 44 Glunz PW, Mueller L, Cheney DL, et al. Atropisomer Control in Macrocyclic Factor VIIa Inhibitors. *J. Med. Chem.* 2016;59:4007–4018. <https://doi.org/10.1021/acs.jmedchem.6b00244>.
- 45 Yamaguchi ST, Tamura Y, Ogata Y, et al. Design and Synthesis of 2-(1-Alkylaminoalkyl)pyrazolo[1,5-a]pyrimidines as New Respiratory Syncytial Virus Fusion Protein Inhibitors. *Chem. Pharm. Bull.* 2020;68:345–362. <https://doi.org/10.1248/cpb.c19-00895>.
- 46 Kanuma K, Kawaguchi T, Kurosaka J, Yamaguchi T, Ogata Y, Iwakiri K. Pyrazolo [1,5-a]pyrimidine Compound. World Intellectual Property Organization, WO/2016/148145, 2016.
- 47 Perrin CL, Dwyer TJ. Application of two-dimensional NMR to kinetics of chemical exchange. *Chem. Rev.* 1990;90:935–967. <https://doi.org/10.1021/cr00104a002>.
- 48 Cronin L, Higgitt CL, Perutz RN. Structure and Dynamic Exchange in Rhodium η^2 -Naphthalene and Rhodium η^2 -Phenanthrene Complexes: Quantitative NOESY and EXSY Studies. *Organometallics.* 2000;19:672–683. <https://doi.org/10.1021/om9908377>.
- 49 Molecular Operating Environment (MOE), 2019.01; Chemical Computing Group Inc., 1010 Sherbooke St. West, Suite #910, Montreal, QC, Canada, H3A 2R7, 2019.
- 50 Dassault Systèmes BIOVIA, Discovery Studio Modeling Environment, Release 2017, San Diego: Dassault Systèmes, 2017.